Free Radical Research

ISSN: 1071-5762 (Print) 1029-2470 (Online) Journal homepage: https://www.tandfonline.com/loi/ifra20

Inhibitors of the protein–protein interaction between phosphorylated p62 and Keap1 attenuate chemoresistance in a human hepatocellular carcinoma cell line

Daisuke Yasuda, Tomoyuki Ohe, Kyoko Takahashi, Riyo Imamura, Hirotatsu Kojima, Takayoshi Okabe, Yoshinobu Ichimura, Masaaki Komatsu, Masayuki Yamamoto, Tetsuo Nagano & Tadahiko Mashino

Inhibitors of the protein-protein interaction between phosphorylated p62 and Keap1 attenuate chemoresistance in a human hepatocellular carcinoma cell line

Daisuke Yasuda[a], Tomoyuki Ohe[a*], Kyoko Takahashi[a], Riyo Imamura[b], Hirotatsu Kojima[b], Takayoshi Okabe[b], Yoshinobu Ichimura[c], Masaaki Komatsu[c], Masayuki Yamamoto[d], Tetsuo Nagano[b] and Tadahiko Mashino[a*].

[a]*Department of Pharmaceutical Sciences, Faculty of Pharmacy, Keio University, 1-5-30 Shibakoen, Minato-ku, Tokyo, Japan*
[b]*Drug Discovery Initiative, The University of Tokyo, 7-3-1 Hongo, Bunkyo-ku, Tokyo, Japan*
[c]*Department of Physiology, Juntendo University School of Medicine, 2-1-1 Hongo, Bunkyo-ku, Tokyo, Japan*
[d]*Department of Medical Biochemistry, Tohoku University School of Medicine, 2-1 Seiryo-machi, Aoba-ku, Sendai-shi, Miyagi, Japan*

* Corresponding authors. Tel.: +81 3 5400 2691; fax +81 3 5400 2691 (T.O.); tel.: +81 3 5400 2694; fax +81 3 5400 2691 (T.M.). E-mail addresses: ohe-tm@pha.keio.ac.jp (T.O.), mashino-td@pha.keio.ac.jp (T.M.)

Abstract
Resistance to anticancer agents has been an obstacle to developing therapeutics and reducing medical costs. Whereas sorafenib is used for the treatment of human hepatocellular carcinoma (HCC), resistance limits its efficacy. p62, a multifunctional protein, is overexpressed in several HCC cell lines, such as Huh-1 cells. Phosphorylated p62 (*p*-p62) inhibits the protein-protein interaction (PPI) between Keap1 and Nrf2, resulting in the Nrf2 overactivation that causes drug resistance. We have found a unique Nrf2 inactivator, named K67, that inhibited the PPI between Keap1 and *p*-p62 and attenuated sorafenib resistance in Huh-1 cells. Herein, we designed and synthesized novel K67 derivatives by modification of the substituent at the 4-position of the two benzenesulfonyl groups of K67. Although these new derivatives inhibited the Keap1-*p*-p62 PPI to a level comparable to or weaker than that of K67, the isopropoxy derivative enhanced the sensitivity of Huh-1 cells to sorafenib to a greater extent than K67 without any influence on the viability of Huh-7 cells, which is a nonresistant HCC cell line. The isopropoxy derivative also increased the sensitivity of Huh-1 cells to regorafenib, which suggests that this derivative has the potential to be used as an agent to overcome chemoresistance based on Nrf2 inactivation.

Keywords: Keap1, Nrf2, p62, protein-protein interaction, chemoresistance

Introduction

Hepatocellular carcinoma (HCC) is the most common liver cancer that develops through liver cirrhosis and is induced by various factors, such as hepatitis B and C viruses, alcohol, mycotoxicins and non-alcoholic fatty liver disease [1]. Hepatectomy, radiofrequency ablation and transarterial chemoembolization are often selected as therapeutics for early-stage HCC[2]. In addition, sorafenib (Figure 1), an oral multikinase inhibitor, is approved as a molecular targeted drug against advanced HCC in more than 70 countries [3]. Sorafenib inhibits the Ras/Raf/MEK/ERK serine/threonine kinase cascade and the tyrosine kinases involved in angiogenesis, such as VEGFR-1/2/3, PDGFRβ, Flt3 and RET, to exert its antitumor activity [4]. However, primary or acquired resistance to sorafenib is sometimes observed in HCC patients [5]. Recently, as a second-line treatment for sorafenib-ineffective patients, regorafenib (Figure 1), an alternative multikinase inhibitor, has been approved. Regorafenib improves the outcomes of highly advanced HCC patients [6], but due to its adverse events and high structural similarity to sorafenib, a novel type of anti-HCC medicine is strongly desired.

p62/sequestosome1 (hereafter referred to as p62) is a stress-induced multifunctional protein that is involved in selective autophagy as a receptor protein and in cell survival or death via the activation of signaling cascades, such as the TRAF6/NF-κB pathway [7]. In a selective autophagy under normal conditions, p62 is localized to ubiquitin-positive aggregated proteins and damaged mitochondria and bacteria via its ubiquitin-associated domain on the C-terminal side, resulting in degradation by autophagosomes [8]. However, p62 is abnormally accumulated in autophagy-deficient cancer cells, including some types of human HCC [9].

p62 also has an interaction site that binds to Kelch-like ECH associated protein 1 (Keap1), which is an adapter protein for Cullin 3 ubiquitin ligase and forms a complex with nuclear factor erythroid 2-related factor 2 (Nrf2) [10]. Nrf2 is one of the transcription factors that induce a variety of antioxidant, phase II detoxification, multidrug resistance-related and cellular proliferation proteins in response to oxidative stress or xenobiotics [11]. Keap1 homodimers suppress Nrf2 activity in physiological conditions by forming a protein-protein interaction (PPI) between the DC domains of Keap1 and ETGE or the DLGex motif of Nrf2, resulting in ubiquitination of the Keap1-Nrf2 complex and, ultimately, degradation of the protein by the 26S proteasome [12]. However, once the sensor thiol group on a specific cysteine residue of Keap1 is modified by oxidative stress or electrophiles, Keap1 partly dissociates from Nrf2, which causes the accumulation of free form Nrf2 followed by the translocation of Nrf2 to the nucleus [13]. The translocated Nrf2 binds to antioxidant response element in a complex with small Maf factor and induces various cellular defensive proteins [13]. Moreover, small molecules that inhibit the PPI between Keap1 and Nrf2 can directly activate Nrf2. This type of small molecule is expected to be a therapeutic agent against oxidative stress-related disorders without off-target effects, and various Keap1-Nrf2 PPI inhibitors have been discovered through a high-throughput screening or fragment-based drug design [14]. The interaction region on p62 to Keap1 has a relatively low affinity, but phosphorylation of Ser351 on murine p62 (corresponding to Ser349 in human) increases its affinity more than 30-fold in comparison with nonphosphorylated p62 [15]. The phosphorylated p62 (*p*-p62) competes with Nrf2 for the Keap1-DC domain just like Keap1-Nrf2 PPI inhibitors, resulting in Nrf2 activation [15]. In autophagy-deficient tumor cells, overaccumulation of *p*-p62 causes constitutive Nrf2 activation and induction of cellular defensive proteins, which leads to tumor progression and gain of chemoresistance [16].

In a previous study, we demonstrated that *p*-p62 promotes chemoresistance to sorafenib and cell growth in HCV-positive HCC via the reprogramming of glucose and glutamine metabolism due to the constitutive Nrf2 activation associated with the overaccumulation of p62 and acceleration of its phosphorylation [16]. This phenomenon was also observed in a human HCC cell line, Huh-1, that is resistant to sorafenib[16]. Additionally, we discovered a selective Keap1-*p*-p62 PPI inhibitor, called K67 (Figure 1), from high-throughput screening using a chemical library that possesses 155,000 compounds [16]. Co-administration of K67 and sorafenib or cisplatin increased the sensitivity of Huh-1 cells to these drugs, whereas Cpd16 (Figure 1), a Keap1-Nrf2 PPI inhibitor that has a similar structure to K67, did not show such effects [16]. X-ray co-crystal analysis of the PPI between K67 and the Keap1-DC domain suggested that the acetonyl group at the 2-position of the naphthalene ring of K67 is important for selective Keap1-*p*-P62 PPI inhibition [16]. We also demonstrated that substitution of the acetonyl group with hydrophilic carboxylates decreased the selectivity towards the PPI between *p*-p62 and Keap1 [17]. Herein, we reported the development of more effective agents to overcome drug resistance in HCC. To this end, we designed and synthesized novel K67 derivatives in which the 4-ethoxybenzenesulfonamide group of K67 was replaced with various 4-substituted benzenesulfonamides. Then, the potential of these derivatives to attenuate chemoresistance in Huh-1 cells was also evaluated.

Materials and Methods

General

^{1}H NMR spectra (500 MHz) were measured on a Varian-500 FT-NMR (Agilent Technologies, USA) with tetramethylsilane as an internal standard (δ=0.00). ^{1}H NMR spectra (600 MHz) were measured on a JEOL JNM-ECP600 FT-NMR (JEOL, Japan) with tetramethylsilane as an internal standard (δ=0.00). ^{13}C NMR spectra (150 MHz) were measured on a JEOL JNM-ECP600 FT-NMR, and the chemical shifts were compared to the signals of DMSO-*d*^{6} (δ=39.50). Mass spectra were recorded on a JEOL JMS-T100LP AccuTOF LC-plus 4G mass spectrometer (ESI-MS). Palladium-catalyzed hydrogenation was performed at ordinary pressure using a balloon. Benzenesulfonyl chloride, 4-chlorobenzensulfonyl chloride, 4-methylbenzensulfonyl chloride, 4-isopropoxybenzenesulfonyl chloride, 4-nitro-1-naphtylamine and 4-propylbenzenesulfonyl chloride were purchased from Tokyo Chemical Industry Co., Ltd. (Japan). Anhydrous sodium sulfate, cerium(IV) ammonium nitrite, 4-ethylbenzensulfonyl chloride and triethylamine were purchased from FUJI FILM Wako Pure Chemical Corp. (Japan). Palladium on charcoal was purchased from Kokusan Chemical Co., Ltd. (Japan).

Chemistry

*1 Preparation of 1,4-bis-[(benzenesulfonyl)amino]naphthalenes (**2c-m**)*

1-1 General procedure

Commercially available 4-nitro-1-naphthylamine was reduced by palladium-catalyzed hydrogenation to **1** according to our previous method [17]. To a solution of **1** (500 mg, 3.16 mmol) in dichloromethane (6 mL), the corresponding benzensulfonyl chloride (2.0 mol equiv.) and pyridine (1 mL) were added. The reaction mixture was stirred at room temperature for 2 hr, and then acidified with 2 M hydrochloric acid and extracted twice with ethyl acetate. The combined organic layer was washed twice with water and twice with brine, dried over anhydrous sodium sulfate and concentrated under reduced pressure.

*1-2 1,4-bis-[(4-n-propoxybenzenesulfonyl)amino]naphthalene (**2c**)*

The pink solid (1.69 g, 97% yield) was obtained. ^{1}H NMR (DMSO-d^{6}, 500 MHz, δ) 0.95 (t, -$OCH^{2}CH^{2}C\underline{H}^{3}$ x2, *J*=7.3 Hz, 6H), 1.70 (m, -$OCH^{2}C\underline{H}^{2}CH^{3}$ x2, 4H), 3.94 (t, -$OC\underline{H}^{2}CH^{2}CH^{3}$ x2, *J*=6.6 Hz, 4H), 6.97 (d, Ar H, *J*=9.0 Hz, 4H), 7.02 (s, Ar H, 2H), 7.39 (dd, Ar H, *J*=6.6, 3.2 Hz, 4H), 7.53 (d, Ar H, *J*=9.0 Hz, 4H), 7.96 (dd, Ar H, *J*=6.6, 3.2 Hz, 2H), 10.02 (brs, 2H, -NH-). LRMS-ESI (*m/z*): 553 [M–H]$^{-}$. HRMS-ESI (*m/z*): [M–H]$^{-}$ calcd for $C^{28}H^{29}N^{2}O^{6}S^{2}$, 553.1467; found, 553.1498 (+3.1 mmu).

*1-3 1,4-bis-[(4-isopropoxybenzenesulfonyl)amino]naphthalene (**2d**)*

The pink solid (1.77 g, quantitative yield) was obtained. ^{1}H NMR (DMSO-d^{6}, 500 MHz, δ) 1.15 (d, -$OCH(C\underline{H}^{3})^{2}$, *J*=6.8 Hz, 12H), 2.90 (*sept*, -$OC\underline{H}(CH^{3})^{2}$, *J*=6.8 Hz, 2H), 7.09 (s, Ar H, 2H), 7.29 (dd, Ar H, *J*=6.6, 3.2 Hz, 2H), 7.32 (d, Ar H, *J*=8.3 Hz, 4H), 7.53 (d, Ar H, *J*=8.3 Hz, 4H), 7.81 (dd, Ar H, *J*=6.6, 3.2 Hz, 2H), 10.13 (brs, 2H, -NH-). LRMS-ESI (*m/z*): 521 [M–H]$^{-}$. HRMS-ESI (*m/z*): [M–H]$^{-}$ calcd for $C^{28}H^{29}N^{2}O^{4}S^{2}$, 521.1569; found, 521.1557 (–1.2 mmu).

*1-4 1,4-bis-[(4-n-butoxybenzenesulfonyl)amino]naphthalene (**2e**)*

The pink solid (1.77 g, 96% yield) was obtained. ^{1}H NMR (DMSO-d^{6}, 500 MHz, δ) 0.98 (t, -$OCH^{2}CH^{2}CH^{2}C\underline{H}^{3}$, *J*=7.3 Hz, 6H), 1.42-1.52 (m, -$OCH^{2}CH^{2}C\underline{H}^{2}CH^{3}$, 2H), 1.79-1.83 (m, -$OCH^{2}C\underline{H}^{2}CH^{2}CH^{3}$, 2H), 4.10 (d, -$OC\underline{H}^{2}CH^{2}CH^{2}CH^{3}$, *J*=6.7 Hz, 6H), 7.04 (s, Ar H, 2H), 7.33 (d, Ar H, *J*=8.3 Hz, 4H), 7.36 (dd, Ar H, *J*=6.6, 3.2 Hz, 2H), 7.53 (d, Ar H, *J*=8.3 Hz, 4H), 7.90 (dd, Ar H, *J*=6.6, 3.2 Hz, 2H), 10.10 (brs, 2H, -NH-). LRMS-ESI (*m/z*): 581 [M+H]$^{+}$. HRMS-ESI (*m/z*): [M+H]$^{+}$ calcd for $C^{30}H^{33}N^{2}O^{6}S^{2}$, 581.1780; found, 581.1781 (+0.1 mmu).

*1-5 1,4-bis-[(4-isobutoxybenzenesulfonyl)amino]naphthalene (**2f**)*

The pink solid (1.78 g, 97% yield) was obtained. ^{1}H NMR (DMSO-d^{6}, 500 MHz, δ) 1.04 (d, -$OCH^{2}CH\ (C\underline{H}^{3})^{2}$, *J*=6.8 Hz, 6H), 2.14 (sept, -$OCH^{2}C\underline{H}\ (CH^{3})^{2}$, *J*=6.8 Hz, 1H), 3.88 (d, -$OC\underline{H}^{2}CH\ (CH^{3})^{2}$, *J*=6.8 Hz, 6H), 7.03 (s, Ar H, 2H), 7.21 (d, Ar H, *J*=8.3 Hz, 4H), 7.34 (dd, Ar H, *J*=6.6, 3.2 Hz, 2H), 7.55 (d, Ar H, *J*=8.3 Hz, 4H), 7.94 (dd, Ar H, *J*=6.6, 3.2 Hz, 2H), 10.12 (brs, 2H, -NH-). LRMS-ESI (*m/z*): 581 [M+H]$^{+}$. HRMS-ESI (*m/z*): [M+H]$^{+}$ calcd for $C^{30}H^{33}N^{2}O^{6}S^{2}$, 581.1780; found, 581.1777 (–0.4 mmu).

*1-6 1,4-bis-[(benzenesulfonyl)amino]naphthalene (**2h**)*

The pink solid (1.35 g, 97% yield) was obtained. ^{1}H NMR (DMSO-d^{6}, 500 MHz, δ) 7.03 (s, Ar H, 2H), 7.35 (dd, Ar H, *J*=6.6, 3.3 Hz, 2H), 7.47 (dd, Ar H, *J*=7.8, 7.6 Hz, 4H), 7.58 (dd, Ar H, *J*=7.6, 7.3 Hz, 2H), 7.61-7.63 (m, Ar H,4H), 7.90 (dd, Ar H, *J*=6.6, 3.3 Hz, 2H), 10.22 (brs, 2H, -NH-). LRMS-ESI (*m/z*): 437 $[M–H]^-$. HRMS-ESI (*m/z*): $[M–H]^-$ calcd for $C_{22}H_{17}N_2O_4S_2$, 437.0630; found, 437.0647 (+1.7 mmu).

*1-7 1,4-bis-[(4-methylbenzenesulfonyl)amino]naphthalene (**2i**)*

The pink solid (1.40 g, 96% yield) was obtained. ^{1}H NMR (DMSO-d_6, 500 MHz, δ) 2.32 (s, $-CH_3$, 6H), 6.99 (s, Ar H, 2H), 7.28 (d, Ar H, *J*=7.8 Hz, 4H), 7.50 (dd, Ar H, *J*=6.6, 3.2 Hz, 2H), 7.52 (d, Ar H, *J*=7.8 Hz, 4H), 7.96 (dd, Ar H, *J*=6.6, 3.2 Hz, 2H), 10.11 (brs, 2H, -NH-). LRMS-ESI (*m/z*): 465 $[M–H]^-$ HRMS-ESI (*m/z*): $[M–H]^-$ calcd for $C_{24}H_{21}N_2O_4S_2$, 465.0943; found, 465.0932 (–1.1 mmu).

*1-8 1,4-bis-[(4-ethylbenzenesulfonyl)amino]naphthalene (**2j**)*

The pink solid (1.52 g, 97% yield) was obtained. ^{1}H NMR (DMSO-d_6, 500 MHz, δ) 1.13 (t, $-CH_2C\underline{H}_3$, *J*=7.6 Hz, 6H), 2.61 (q, $-C\underline{H}_2CH_3$, *J*=7.6 Hz, 4H), 7.04 (s, Ar H, 2H), 7.30 (d, Ar H, *J*=8.3 Hz, 4H), 7.33 (dd, Ar H, *J*=6.6, 3.2 Hz, 2H), 7.53 (d, Ar H, *J*=8.3 Hz, 4H), 7.89 (dd, Ar H, *J*=6.6, 3.2 Hz, 2H), 10.12 (brs, 2H, -NH-). LRMS-ESI (*m/z*): 493 $[M–H]^-$. HRMS-ESI (*m/z*): $[M–H]^-$ calcd for $C_{26}H_{25}N_2O_4S_2$, 493.1256; found, 493.1235 (–2.1 mmu).

*1-9 1,4-bis-[(4-n-propylbenzenesulfonyl)amino]naphthalene (**2k**)*

The pink solid (1.32 g, 70% yield) was obtained. ^{1}H NMR (DMSO-d_6, 500 MHz, δ) 0.19 (t, $-CH_2CH_2C\underline{H}_3$, *J*=7.3 Hz, 6H), 1.53 (*sext*, $-CH_2C\underline{H}_2CH_3$,, *J*=7.3 Hz, 4H), 2.56 (*t*, $-C\underline{H}_2CH_2CH_3$,, *J*=7.3 Hz, 4H),7.04 (s, Ar H, 2H), 7.27 (d, Ar H, *J*=8.1 Hz, 4H), 7.31 (dd, Ar H, *J*=6.6, 3.2 Hz, 2H), 7.51 (d, Ar H, *J*=8.3 Hz, 4H), 7.85 (dd, Ar H, *J*=6.6, 3.2 Hz, 2H), 10.13 (brs, 2H, -NH-). LRMS-ESI (*m/z*): 521 $[M–H]^-$. HRMS-ESI (*m/z*): $[M–H]^-$ calcd for $C_{28}H_{29}N_2O_4S_2$, 521.1569; found, 521.1560 (–0.9 mmu).

*1-10 1,4-bis-[(4-isopropylbenzenesulfonyl)amino]naphthalene (**2l**)*

The pink solid (1.65 g, quantitative yield) was obtained. ^{1}H NMR (DMSO-d_6, 500 MHz, δ) 1.15 (d, $-OCH(C\underline{H}_3)_2$, *J*=6.8 Hz, 12H), 2.90 (*sept*, $-OC\underline{H}(CH_3)_2$, *J*=6.8 Hz, 2H), 7.09 (s, Ar H, 2H), 7.29 (dd, Ar H, *J*=6.6, 3.2 Hz, 2H), 7.32 (d, Ar H, *J*=8.3 Hz, 4H), 7.53 (d, Ar H, *J*=8.3 Hz, 4H), 7.81 (dd, Ar H, *J*=6.6, 3.2 Hz, 2H), 10.13 (brs, 2H, -NH-). LRMS-ESI (*m/z*): 521 $[M–H]^-$. HRMS-ESI (*m/z*): $[M–H]^-$ calcd for $C_{28}H_{29}N_2O_4S_2$, 521.1569; found, 521.1557 (–1.2 mmu).

*1-11 1,4-bis-[(4-chlorobenzenesulfonyl)amino]naphthalene (**2m**)*

The pink solid (1.77 g, 96% yield) was obtained. ^{1}H NMR (DMSO-d_6, 500 MHz, δ) 7.04 (s, Ar H, 2H), 7.41 (dd, Ar H, *J*=6.6, 3.2 Hz, 2H), 7.56 (dd, Ar H, *J*=6.8, 2.2 Hz, 4H), 7.62 (dd, Ar H, *J*=6.8, 2.2 Hz, 4H), 7.92 (dd, Ar H, *J*=6.6, 3.2 Hz, 2H), 10.33 (brs, 2H, -NH-). LRMS-ESI (*m/z*): 504, 506 $[M–H]^-$. HRMS-ESI (*m/z*): $[M–H]^-$ calcd for $C_{22}H_{15}{}^{35}Cl_2N_2O_4S_2$, 504.9850; found, 504.9836 (–1.4 mmu).

*2 Preparation of 2-acetonyl-1,4-bis-[(benzenesulfonyl)amino]naphthalenes (**5c-5f** and **5h-5m**)*

2-1 General procedure

(1) To a suspension of the obtained product (**2c-2f** and **2h-2m**, 600 mg) in methanol (30 mL), cerium(IV) ammonium nitrite (2.2 equiv.) was added, and the reaction mixture was stirred at room temperature for 30 min. Then, the precipitates were collected by filtration and dried *in vacuo*. (2) To a suspension of the obtained product in toluene (30 mL), *para*-methoxybenzyl acetoacetate (1.1 equiv.) and triethyamine (5.0 equiv.) were added. The reaction mixture was stirred at room temperature for 30 min. Then, the reaction was quenched with 2 M hydrochloric acid and was extracted twice with ethyl acetate. The combined organic layer was washed twice with water and twice with brine, dried over anhydrous sodium sulfate, and concentrated under reduced pressure. (3) The obtained compound was dissolved in trifluoroacetic acid and stirred at room temperature for 30 min. Then, the reaction mixture was poured into water (*ca*. 200 mL), and the precipitates were collected by filtration and dried *in vacuo*. The crude product in the residue was purified with MPLC (*n*-hexane/ethyl acetate gradient).

*2-2 2-Acetonyl-1,4-bis-[(4-n-propoxybenzenesulfonyl)amino]naphthalene (**5c**)*

The yellow solid (162 mg, 32% yield over 3 steps) was obtained. Recrystallization from *n*-hexane/ethyl acetate gave colorless needles. ^{1}H NMR (DMSO-d^{6}, 600 MHz, δ) 0.94 (t, *J*=7.1 Hz, -OCH^{2}CH^{2}C$\underline{H}^3$, 3H), 0.96 (t, *J*=7.1 Hz, -OCH^{2}CH^{2}C$\underline{H}^3$, 3H), 1.66-1.74 (m, -OCH^{2}C$\underline{H}^2$CH^3 x2, 4H), 2.02 (s, -COCH^3, 3H), 3.79 (brs, -CH^{2}CO-, 2H), 3.93-3.96 (m, -OC$\underline{H}^2$CH^{2}CH^3 x2, 4H), 6.92 (d, *J*=8.8 Hz, Ar H, 2H), 6.97 (d, *J*=8.8 Hz, Ar H, 2H), 7.06 (s, Ar H, 1H), 7.15 (dd, *J*=8.2, 7.2 Hz, Ar H, 1H), 7.29 (dd, *J*=8.2, 7.2 Hz, Ar H, 1H), 7.39 (d, J=8.8 Hz, Ar H, 1H), 7.50 (d, *J*=8.3 Hz, Ar H, 1H), 7.91 (d, *J*=8.3 Hz, Ar H, 1H), 9.74 (brs, -NH-, 1H), 10.09 (brs, -NH-, 1H). ^{13}C NMR (DMSO-d^{6}, 150 MHz, δ) 10.21, 21.72, 21.75, 29.66, 46.01, 69.40, 69.42, 114.54, 114.66, 122.92, 124.01, 125.37, 125.61, 125.69, 128.55, 128.73, 128.83, 128.91, 131.22, 131.77, 131.98, 132.65, 161.75, 161.85, 204.74. LRMS-ESI (*m/z*): 609 [M–H]$^-$. HRMS-ESI (*m/z*): [M–H]$^-$ calcd for C^{31}H^{33}N^{2}O^{7}S^2, 609.1729; found, 609.1742 (+1.2 mmu).

*2-3 2-Acetonyl-1,4-bis-[(4-isopropoxybenzenesulfonyl)amino]naphthalene (**5d**)*

The yellow solid (254 mg, 43% yield over 3 steps) was obtained. Recrystallization from *n*-hexane/ethyl acetate gave colorless needles. ^{1}H NMR (DMSO-d^{6}, 600 MHz, δ) 1.22-1.25 (m, -(CH^3)^2 x2, 12H), 3.80 (brs, -CH^{2}CO-, 2H), 4.65-4.66 (m, -CH- x2, 2H), 6.89 (dd, *J*=8.8, 2.2 Hz, Ar H, 2H), 6.94 (dd, *J*=8.8, 2.2 Hz, Ar H, 2H), 7.06 (s, Ar H, 1H), 7.09-7.12 (m, Ar H, 1H), 7.24-7.27 (m, Ar H, 1H), 7.35 (dd, *J*=8.8, 2.2 Hz, Ar H, 2H), 7.47 (d, *J*= 8.8 Hz, Ar H, 1H), 7.55 (dd, *J*=8.8, 2.2 Hz, Ar H, 2H), 7.88 (d, *J*= 8.8 Hz, Ar H, 1H), 9.73 (brs, -NH-, 1H), 10.07 (brs, -NH-, 1H). ^{13}C NMR (DMSO-d^{6}, 150 MHz, δ) 21.45, 21.48, 29.63, 46.15, 69.79, 69.82, 115.39, 115.56, 122.89, 123.95, 125.27, 125.59, 125.79, 128.60, 128.75, 128.86, 128.93, 130.92, 131.41, 131.94, 132.68, 160.64, 160.72, 204.72. LRMS-ESI (*m/z*): 609 [M–H]$^-$. HRMS-ESI (*m/z*): [M–H]$^-$ calcd for C^{31}H^{33}N^{2}O^{7}S^2, 609.1729; found, 609.1736 (+0.7 mmu).

*2-4 2-Acetonyl-1,4-bis-[(4-n-butoxybenzenesulfonyl)amino]naphthalene (**5e**)*

The yellow solid (394 mg, 52% yield over 3 steps) was obtained. Recrystallization from *n*-hexane/ethyl acetate gave colorless needles. ^{1}H NMR (DMSO-d^6, 600 MHz, δ) 0.90 (t, *J*=7.1 Hz, -$OCH^2CH^2CH^2C\underline{H}^3$, 3H), 0.93 (t, *J*=7.1 Hz, -$OCH^2CH^2CH^2C\underline{H}^3$, 3H), 1.36-1.44 (m, -$OCH^2CH^2C\underline{H}^2CH^3$ x2, 4H), 1.64-1.70 (m, -$OCH^2C\underline{H}^2CH^2CH^3$ x2, 4H), 2.01 (s, -$COCH^3$, 3H), 3.78 (brs, -CH^2CO-, 2H), 3.96-4.00 (m, -$OC\underline{H}^2CH^2CH^2CH^3$, 4H), 6.92 (d, *J*=8.8 Hz Ar H, 2H), 6.96 (d, *J*=8.8 Hz Ar H, 2H), 7.05 (s, Ar H, 1H), 7.12-7.15 (m, Ar H, 1H), 7.26-7.29 (m, Ar H, 1H), 7.38 (d, *J*=8.8 Hz Ar H, 2H), 7.49 (d, *J*=8.3 Hz, Ar H, 1H), 7.57 (d, *J*=8.8 Hz Ar H, 2H), 7.91 (d, *J*=8.3 Hz, Ar H, 1H), 9.72 (brs, -NH-, 1H), 10.08 (brs, -NH-, 1H). ^{13}C NMR (DMSO-d^6, 150 MHz, δ) 13.60, 13.61, 18.59, 29.64, 30.38, 30.43, 46.16, 67.67, 114.52, 114.65, 122.95, 123.99, 125.27, 125.64, 128.72, 128.83, 128.88, 131.79, 132.00, 132.66, 161.71, 161.86, 204.77. LRMS-ESI (*m/z*): 637 [M–H]$^-$. HRMS-ESI (*m/z*): [M–H]$^-$ calcd for $C^{33}H^{37}N^2O^7S^2$, 637.2042; found, 637.2031 (–1.1 mmu).

*2-5 2-Acetonyl-1,4-bis-[(4-isobutoxybenzenesulfonyl)amino]naphthalene (**5f**)*

The yellow solid (426 mg, 38% yield over 3 steps) was obtained. Recrystallization from *n*-hexane/ethyl acetate gave colorless needles. ^{1}H NMR (DMSO-d^6, 600 MHz, δ) 0.94 (d, *J*=6.6 Hz, -$OCH^2CH(C\underline{H}^3)^2$, 6H), 0.96 (d, *J*=6.6 Hz, -$OCH^2CH(C\underline{H}^3)^2$, 6H), 1.95-2.03 (m, -$OCH^2C\underline{H}(CH^3)^2$, 2H), 2.01 (s, -$COCH^3$, 3H), 3.76 (d, *J*=6.6 Hz, -$OC\underline{H}^2CH(CH^3)^2$, 2H), 3.76 (brs, -$CH^2CO$-, 2H), 3.77 (d, *J*=6.6 Hz, -$OC\underline{H}^2CH(CH^3)^2$, 2H), 6.93 (d, *J*=8.8 Hz, Ar H, 2H), 6.98 (d, *J*=8.8 Hz, Ar H, 2H), 7.06 (s, Ar H, 1H), 7.14 (dd, *J*=8.2, 7.2 Hz, Ar H, 1H), 7.28 (dd, *J*=8.2, 7.2 Hz, Ar H, 1H), 7.38 (d, *J*=8.8 Hz, Ar H, 2H), 7.50 (d, *J*=8.2 Hz, Ar H, 1H), 7.58 (d, *J*=8.8 Hz, Ar H, 2H), 7.92 (d, *J*=8.2 Hz, Ar H, 1H), 9.74 (brs, -NH-, 1H), 10.09 (brs, -NH-, 1H). ^{13}C NMR (DMSO-d^6, 150 MHz, δ) 18.86, 27.46, 27.51, 29.65, 46.14, 74.06, 74.10, 114.58, 114.71, 122.92, 124.00, 125.33, 125.50, 125.68, 128.49, 128.71, 128.81, 128.91, 131.27, 131.80, 132.00, 132.65, 161.83, 161.97, 204.72. LRMS-ESI (*m/z*): 637 [M–H]$^-$. HRMS-ESI (*m/z*): [M–H]$^-$ calcd for $C^{33}H^{37}N^2O^7S^2$, 637.2042; found, 637.2030 (–1.2 mmu).

*2-6 2-Acetonyl-1,4-bis-[(benzenesulfonyl)amino]naphthalene (**5h**)*

The yellow solid (255 mg, 38% yield over 3 steps) was obtained. Recrystallization from *n*-hexane/ethyl acetate gave colorless needles. ^{1}H NMR (DMSO-d^6, 600 MHz, δ) 2.01 (s, -$COCH^3$, 3H), 3.78 (brs, -CH^2CO-, 2H), 7.08 (s, Ar H, 1H), 7.11 (dd, *J*=8.2, 7.2 Hz, Ar H, 1H), 7.26 (dd, *J*=8.2, 7.2 Hz, Ar H, 1H), 7.44-7.60 (m, Ar H, 9H), 7.68 (d, *J*=7.7 Hz, 2H), 7.87 (d, *J*=8.8 Hz, Ar H, 1H), 9.95 (brs, -NH-, 1H), 10.29 (brs, -NH-, 1H). ^{13}C NMR (DMSO-d^6, 150 MHz, δ) 29.71, 46.08, 122.85, 123.87, 125.51, 125.82, 126.04, 126.54, 126.67, 128.61, 128.87, 129.06, 129.18, 131.51, 131.96, 132.76, 132.78, 139.76, 140.29, 204.63. LRMS-ESI (*m/z*): 493 [M–H]$^-$. HRMS-ESI (*m/z*): [M–H]$^-$ calcd for $C^{25}H^{21}N^2O^5S^2$, 493.0892; found, 493.0913 (+2.1 mmu).

*2-7 2-Acetonyl-1,4-bis-[(4-methylbenzenesulfonyl)amino]naphthalene (**5i**)*

The yellow solid (306 mg, 43% yield over 3 steps) was obtained. Recrystallization from *n*-hexane/ethyl acetate gave colorless needles. ^{1}H NMR (DMSO-d^6, 600 MHz, δ) 1.99 (s, -$COCH^3$, 3H), 2.31 (s, -CH^3, 3H), 2.30 (s, -CH^3, 3H), 3.74 (brs, -CH^2CO-. 2H), 7.05 (s, Ar H, 1H), 7.13-7.16 (m, Ar H, 1H), 7.24-7.31 (m, Ar H, 5H), 7.39 (d, *J*=8.3 Hz, Ar H, 2H), 7.50 (d, *J*=8.8 Hz, Ar H, 1H), 7.56 (d, *J*=8.3 Hz, Ar H, 2H), 7.91 (d, *J*=8.8 Hz, Ar H, 1H), 9.82 (brs, -NH-, 1H), 10.19 (brs, -NH-, 1H). ^{13}C NMR (DMSO-d^6, 150 MHz, δ) 20.93, 29.05, 29.62, 46.08, 122.89, 124.01, 125.45, 125.77, 126.59, 126.73, 128.47, 128.78, 129.45, 129.52, 131.62, 132.05, 132.65, 137.03, 137.58, 142.98, 143.04, 204.68. LRMS-ESI (*m/z*): 521 [M–H]$^-$. HRMS-ESI (*m/z*): [M–H]$^-$ calcd for $C^{27}H^{25}N^2O^5S^2$, 521.1205; found, 521.1182 (–2.3 mmu).

*2-8 2-Acetonyl-1,4-bis-[(ethylbenzenesulfonyl)amino]naphthalene (**5j**)*
The yellow solid (466 mg, 70% yield over 3 steps) was obtained. Recrystallization from *n*-hexane/ethyl acetate gave colorless needles. ^{1}H NMR (DMSO-d^6, 600 MHz, δ) 1.11-1.15 (m, -$CH^2C\underline{H}^3$ x2, 6H), 1.98 (s, -$COCH^3$, 3H), 2.59-2.64 (m, -$C\underline{H}^2CH^3$ x2, 2H), 3.75 (brs, -CH^2CO-, 2H), 7.04 (s, Ar H, 1H), 7.09 (dd, *J*=7.7, 7.2 Hz, Ar H, 1H), 7.23-7.27 (m, Ar H, 3H), 7.30 (d, *J*=8.3 Hz, Ar H, 2H), 7.40 (d, *J*=8.3 Hz, Ar H, 2H), 7.43 (d, *J*=8.2 Hz, Ar H, 1H), 7.57 (d, *J*=8.3 Hz, Ar H, 2H), 7.85 (d, *J*=8.2 Hz, Ar H, 1H), 9.82 (brs. -NH-, 1H), 10.17 (brs, -NH-, 1H). ^{13}C NMR (DMSO-d^6, 150 MHz, δ) 15.14, 15.49, 27.95, 28.03, 29.63, 46.09, 122.87, 123.88, 125.35, 125.66, 125.76, 126.68, 126.83, 128.33, 128.48, 128.58, 128.87, 131.66, 131.99, 132.70, 137.12, 137.59, 149.07, 149.28, 204.64. LRMS-ESI (*m/z*): 549 [M–H]$^-$. HRMS-ESI (*m/z*): [M–H]$^-$ calcd for $C^{29}H^{29}N^2O^5S^2$, 549.1518; found, 549.1530 (+1.2 mmu).

*2-9 2-Acetonyl-1,4-bis-[(4-n-propylbenzenesulfonyl)amino]naphthalene (**5k**)*
The light-yellow solid (303 mg, 46% yield over 3 steps) was obtained. Recrystallization from *n*-hexane/ethyl acetate gave colorless needles. ^{1}H NMR (DMSO-d^6, 600 MHz, δ) 0.82 (t, *J*=7.7 Hz, -$CH^2CH^2C\underline{H}^3$, 3H), 0.85 (t, *J*=7.7 Hz, -$CH^2CH^2C\underline{H}^3$, 3H), 1.50-1.58 (m, -$CH^2C\underline{H}^2CH^3$ x2, 4H), 2.56 (t, *J*=7.7 Hz, -$C\underline{H}^2CH^2CH^3$, 2H), 2.57 (t, *J*=7.7 Hz, -$C\underline{H}^2CH^2CH^3$, 2H), 3.74 (brs, -CH^2CO-, 2H), 7.02 (s, Ar H, 1H), 7.05-7.08 (m, Ar H, 1H), 7.20-7.23 (m, Ar H, 1H), 7.24 (d, *J*=8.3 Hz, Ar H, 2H), 7.27 (d, *J*=8.3 Hz, Ar H, 2H), 7.39 (d, *J*=8.3 Hz, Ar H, 2H), 7.42 (d, *J*=8.8 Hz, Ar H, 1H), 7.55 (d, *J*=8.3 Hz, Ar H, 2H), 7.84 (d, *J*=8.8 Hz, Ar H, 1H), 9.82 (brs, -NH-, 1H), 10.16 (brs. -NH-, 1H). ^{13}C NMR (DMSO-d^6, 150 MHz, δ) 13.36, 13.37, 23.64, 23.83, 29.62, 36.82, 36.87, 46.15, 122.89, 123.83, 125.24, 125.60, 126.59, 126.69, 128.85, 128.94, 129.01, 131.96, 132.71, 137.70, 147.29, 147.51, 204.69. LRMS-ESI (*m/z*): 577 [M–H]$^-$. HRMS-ESI (*m/z*): [M–H]$^-$ calcd for $C^{31}H^{33}N^2O^5S^2$, 577.1831; found, 577.1803 (–2.8 mmu).

*2-10 2-Acetonyl-1,4-bis-[(4-isopropylbenzenesulfonyl)amino]naphthalene (**5l**)*
The yellow solid (152 mg, 23% yield over 3 steps) was obtained. Recrystallization from *n*-hexane/ethyl acetate gave colorless needles. ^{1}H NMR (DMSO-d^6, 600 MHz, δ) 1.15 (d, *J*=7.1 Hz, -$CH(C\underline{H}^3)^2$, 6H), 1.17 (d, *J*=7.1 Hz, -$CH(C\underline{H}^3)^2$, 6H), 1.98 (s, -$COCH^3$, 3H) 2.88-2.96 (m, -$C\underline{H}(CH^3)^2$, 2H), 3.74 (brs, -CH^2CO-, 2H), 7.01 (s, Ar H, 1H), 7.05 (dd, *J*= 8.2, 7.7 Hz, Ar H, 1H), 7.21 (dd, *J*= 8.2, 7.7 Hz, Ar H, 1H), 7.29 (d, *J*=8.2 Hz, Ar H, 2H), 7.33 (d, *J*=8.2 Hz, Ar H, 2H), 7.37 (d, *J*=8.8 Hz, Ar H, 1H), 7.40 (d, *J*=8.2 Hz, Ar H, 2H), 7.56 (d, *J*=8.2 Hz, Ar H, 2H), 7.80 (d, *J*=8.8 Hz, Ar H, 1H), 9.82 (brs, -NH-, 1H), 10.14 (brs, -NH-, 1H). ^{13}C NMR (DMSO-d^6, 150

MHz, δ) 23.42, 23.54, 29.61, 33.33, 33.40, 46.12, 122.86, 123.79, 125.23, 125.55, 125.88, 126.69, 126.83, 126.91, 127.03, 128.95, 131.95, 132.74, 137.21, 137.63, 153.56, 153.81, 204.62. LRMS-ESI (*m/z*): 577 $[M–H]^-$. HRMS-ESI (*m/z*): $[M–H]^-$ calcd for $C_{31}H_{33}N_2O_5S_2$, 577.1831; found, 577.1824 (–0.7 mmu).

*2-11 2-Acetonyl-1,4-bis-[(4-chlorobenzenesulfonyl)amino]naphthalene (**5m**)*

The yellow solid (372 mg, 67% yield over 3 steps) was obtained. Recrystallization from *n*-hexane/ethyl acetate gave colorless needles. ^1H NMR (DMSO-d_6, 600 MHz, δ) 2.05 (s. $-COCH_3$, 3H), 3.85 (brs, $-CH_2CO-$, 2H), 7.09 (s, Ar H, 1H), 7.17 (dd, *J*=8.2, 7.2 Hz, Ar H, 1H), 7.31 (dd, *J*=8.2, 7.2 Hz, Ar H, 1H), 7.45 (d, *J*=8.8 Hz, Ar H, 1H), 7.48-7.52 (m, Ar H, 4H), 7.56 (d, *J*=8.8 Hz, Ar H, 2H), 7.66 (d, *J*=8.8 Hz, Ar H, 2H), 7.87 (d, *J*=8.8 Hz, Ar H, 1H), 10.09 (brs, -NH-, 1H), 10.39 (brs. -NH-, 1H). ^{13}C NMR (DMSO-d_6, 150 MHz, δ) 29.75, 46.09, 122.92, 123.74, 125.69, 125,98, 126.41, 128.50, 128.57, 128.67, 128.94, 129.25, 129.28, 131.34, 131.78, 132.96, 137.66, 137.70, 138.58, 139.97, 204.58. LRMS-ESI (*m/z*): 561, 563 $[M–H]^-$. HRMS-ESI (*m/z*): $[M–H]^-$ calcd for $C_{25}H_{19}{}^{35}Cl_2N_2O_5S_2$, 561.0112; found, 561.0145 (+3.2 mmu).

*3Synthesis of 2-acetonyl-1,4-bis-[4-(hydroxybenzenesulfonyl)amino]naphthalene (**5g**)*

*3-1 Synthesis of 1,4-bis-[4-(benzyloxy)benzenesulfonyl)amino]-naphthalene (**2g**)*

To a solution of **1** (520 mg, 3.29 mmol) in dichloromethane (10 mL), 4-(benzyloxy)benzenesulfonylcholide (1.91 g, 6.77 mmol, 1.0 mol equiv.) and pyridine (2 mL) were added. The reaction mixture was stirred at room temperature for 2 hr and then acidified with 2 M hydrochloric acid, and the precipitates were collected by filtration, washed with dichloromethane, and dried *in vacuo*. A colorless solid (1.97 g, 92% yield) was obtained. ^1H NMR ($CDCl_3$, 500 MHz, δ) 5.04 (s, $-CH_2-$ x2, 4H), 6.62 (s, Ar H, 2H), 6.89 (d, *J*=8.6 Hz, Ar H, 4H), 7.20 (s, Ar H, 2H), 7.41 (s, Ar H,2H), 7.36-7.44 (m, Ar H,10H), 7.61 (d, *J*=8.6 Hz,Ar H, 2H), 7.80-7.82 (m, Ar H, 4H,). LRMS-ESI (*m/z*): 650 $[M–H]^-$. HRMS-ESI (*m/z*): $[M–H]^-$ calcd for $C_{36}H_{30}N_2O_6S_2$, 650.1545; found, 650.1528 (–1.7 mmu).

*3-2 Preparation of 2-acetonyl1,4-bis-[4-(hydroxybenzenesulfonyl)amino]-naphthalene (**5g**)*

(1) To a suspension of the **2g** (1.97 g, 3.03 mmol) in methanol (50 mL), cerium(IV) ammonium nitrite (3.32 g, 6.05 mmol, 2.0 mol equiv.) was added and the reaction mixture was stirred at room temperature for 30 min. Then, the precipitates were collected by filtration and dried *in vacuo*. (2) To a suspension of the obtained product in toluene (40 mL), benzyl acetoacetate (1.0 equiv.) and triethylamine (5.0 equiv.) were added. The reaction mixture was stirred at room temperature for 30 min. Then, the reaction was quenched with 2 M hydrochloric acid and was extracted twice with toluene. The combined organic layer was washed twice with water and twice with brine, dried over anhydrous sodium sulfate, and concentrated under reduced pressure. (3) The obtained compound was dissolved in ethanol, and 5% palladium on charcoal was added to the solution. The reaction mixture was stirred under a hydrogen atmosphere at room temperature for 14 hr. The catalyst was removed by filtration through a Celite® pad, and the solvent was concentrated under reduced pressure. A brown solid (1.26 g, 71% yield over 3 steps) was obtained. Recrystallization

from ethyl acetate gave colorless needles. ^{1}H NMR (DMSO-d^6, 600 MHz, δ) 2.01 (s, -COCH^3, 3H), 3.77 (brs, -CH^{2}CO-, 2H), 6.75-6.77 (m, Ar H, 4H), 7.06 (s, Ar H, 1H), 7.15-7.18 (m, Ar H, 1H), 7.28-7.31 (m, Ar H, 3H), 7.48 (dd, *J*= 7.2, 2.2Hz, Ar H, 2H), 7.54 (d, *J*=8.3 Hz, Ar H, 1H), 7.92 (d, *J*=8.3 Hz, Ar H, 1H), 9.64 (brs, -NH-, 1H), 10.00 (brs, -NH-, 1H), 10.38 (brs, 2H, -OH). ^{13}C NMR (DMSO-d^6, 150 MHz, δ) 29.69, 46.17, 115.33, 115.45, 122.94, 124.17, 125.37, 125.45, 125.68, 128.62, 128.83, 128.92, 129.09, 129.73, 130.39, 131.86, 132.08, 132.62, 161.13, 161.23, 204.88. LRMS-ESI (*m/z*): 549 [M+Na]$^+$. HRMS-ESI (*m/z*): [M+H]$^+$ calcd for $C^{25}H^{22}N^2Na^1O^7S^2$, 631.1297; found, 631.1304 (+0.7 mmu).

*4 Preparation of 2-acetonyl-1,4-bis-{[4-(acethylamino)benzenesulfonyl]amino}naphthalene **(5n)***

*4-1 Preparation of 1,4-bis-{[4-(acethylamino)benzenesulfonyl)amino]naphthalene **(2n)***

To a solution of **1 (**422 mg, 2.67 mmol**)** in dichloromethane (20 mL), 4-acetoaminobenzenesulfonyl chloride (1.40 g, 5.98 mmol, 1.1 mol equiv.) and pyridine (1 mL) were added. The reaction mixture was stirred at room temperature for 3 hr, and then acidified with 2 M hydrochloric acid and extracted twice with ethyl acetate. The combined organic layer was washed twice with brine, dried over anhydrous sodium sulfate and concentrated under reduced pressure. The residues were purified by silica-gel column chromatography yielding a light-purple solid (513 mg, 35% yield). ^{1}H NMR (DMSO-d^6, 500 MHz, δ) 2.06 (s, -CH^3 x2, 6H), 6.97 (s, Ar H, 2H), 7.38 (dd, *J*=6.5, 3.0 Hz, Ar H, 2H), 7.54 (d, *J*=8.8 Hz, Ar H, 4H), 7.67 (d, *J*=8.8 Hz, Ar H, 4H), 7.98 (dd, *J*=6.5, 3.0 Hz, Ar H, 2H), 10.05 (brs, 2H, -NH-), 10.23 (brs, 2H, -NH-). LRMS-ESI (*m/z*): 551 [M–H]$^–$. HRMS-ESI (*m/z*): [M–H]$^–$ calcd for $C^{26}H^{23}N^4O^6S^2$, 551.1059; found, 551.1065 (+0.6 mmu).

*4-2 Preparation of 2-acetonyl-1,4-bis-{[4-(acethylamino)benzenesulfonyl]amino}naphthalene **(5n)***

(1) To a suspension of **2n** (331 mg, 0.599 mmol) in methanol (50 mL), cerium(IV) ammonium nitrite (1.2 equiv.) was added and the reaction mixture was stirred at room temperature for 30 min. Then, the precipitates were collected by filtration and dried *in vacuo*. (2) To a suspension of the obtained product in toluene (30 mL), *para*-methoxybenzyl acetoacetate (1.1 equiv.) and triethylamine (5.0 equiv.) were added. The reaction mixture was stirred at room temperature for 30 min. Then, the reaction was quenched with 2 M hydrochloric acid and was extracted twice with ethyl acetate. The combined organic layer was washed twice with water and twice with brine, dried over anhydrous sodium sulfate, and concentrated under reduced pressure. (3) The obtained compound was dissolved in trifluoroacetic acid and stirred at room temperature for 30 min. Then, the reaction mixture was poured into water (*ca*. 200 mL), and the precipitates were collected by filtration and dried *in vacuo*. Purification of the crude product with MPLC (*n*-hexane/ethyl acetate gradient) produced an off-white solid (64 mg, 18% yield). Recrystallization from ethyl acetate gave colorless plates. ^{1}H NMR (DMSO-d^6, 600 MHz, δ) 2.00 (s, -COCH^3, 3H), 2.05 (s, -COCH^3, 3H), 2.08 (s, -COCH^3, 3H), 3.76 (brs, -CH^{2}CO-, 2H), 7.07 (s, Ar H, 1H), 7.17 (dd, *J*=7.7, 7.1 Hz, Ar H, 1H), 7.30 (dd, *J*=7.7, 7.1 Hz, Ar H, 1H), 7.45 (d, *J*=8.8 Hz, Ar H, 2H), 7.55 (d, *J*=8.2 Hz, Ar H, 1H), 7.60 (d, *J*=8.8 Hz, 2H), 7.63-7.65 (m, Ar H, 4H), 7.92 (d, *J*=8.2 Hz, Ar

H, 1H), 9.80 (brs, -NHSO^{2}-, 1H), 10.15 (brs, -NHSO^{2}-, 1H), 10.25 (s, -NHCO-, 1H), 10.28 (s, -NHCO-, 1H). ^{13}C NMR (DMSO-d^{6}, 150 MHz, δ) 24.14, 24.17, 29.69, 46.12, 118.32, 118.48, 122.94, 124.13, 125.53, 125.83, 127.79, 127.91, 128.60, 128.84, 131.71, 132.09, 132.69, 133.04, 134.11,143.04, 169.00, 204.78. LRMS-ESI (*m/z*): 631 [M+Na]$^{+}$. HRMS-ESI (*m/z*): [M+H]$^{+}$ calcd for $C^{29}H^{28}N^{4}Na^{1}O^{7}S^{2}$, 631.1297; found, 631.1304 (+0.7 mmu).

Determination of the PPI inhibitory activities

FAM-labeled Nrf2 peptide (FAM-LDEETGEFL-NH^{2}) and FAM-labeled *p*-p62 peptide (FAM-VDP-pS-TGELQ-NH2) were purchased from was purchased from Toray Research Center (Tokyo, Japan). GST-His-Keap1-DC (amino acids 321–609) were expressed in *Escherichia coli* and purified by chromatography on glutathione–Sepharose 4B resin (GE Healthcare, USA). GST-His-Keap1-DC was cleaved to His-Keap1-DC with PreScission Protease (GE Healthcare, USA) before use in this assay. Fluorescence polarization assays was performed in 384-well nonbinding black plates (784900 Greiner Bio-One, Austria). Five microliters of 20 nM peptide solution and 5 μL of 500 nM protein solution were diluted with fluorescence polarization (FP) assay buffer (10 mM HEPES, pH 7.4, 0.5 mM EDTA, 150 mM NaCl, 0.5 mM TCEP and 0.005% Tween-20) were dispensed to each well where 100 nL of 1 mM tested compound solution in dimethyl sulfoxide was transferred in advance by an Echo 550 liquid handler (Labcyte, USA). Subsequently, the plates were incubated for 30 min at room temperature. The FP signal was measured at 520 nm with excitation at 485 nm by a PHERAstar plate reader (BMG Labtech, Germany).

Cell culture

Both the Huh-1 and Huh-7 cell lines were purchased from the JCRB cell bank (Japan) and cultured in DMEM (4.5 g/mL glucose) supplemented with 10% fetal bovine serum (Life Technologies, USA) and 1% penicillin-streptomycin (Sigma, USA) at 37°C, 5% CO^{2} and a humidified atmosphere.

Cell viability assay

Both Huh-1 and Huh-7 cells were seeded on 96-well flat bottom plates (AGC Techno Glass, Japan) at a concentration of 5,000 cell/well (total medium volume was 200 μL/well). After 24 hr incubation until adhesion, drug samples diluted in DMSO (1 μL) were added (*n*=3), and the cells were incubated for 72 hr. Then, sorafenib or regorafenib diluted in DMSO (1 μL) were added to the cells, and the cells were incubated for another 72 hr. Next, Cell Counting Kit-8 (Dojindo, Japan) solution (10 μL) was added to each well and incubated for 4 hr, and the absorbance at 450 nm (reference: 600 nm) was measured to calculate the cell viability.

Results

Compound design and synthesis

As mentioned above, the acetonyl group on 2-position of K67 seemed to be essential for selective inhibition of the Keap1-*p*-p62 PPI [17]. However, the effect of the alkoxy group on the 4-position of the two benzenesulfonyl groups of K67 on the PPI inhibition has been rarely investigated. Therefore, we designed new K67 derivatives that have various lengths of alkoxy or alkyl groups at this position. Additionally, hydroxy, chloro and acetamide derivatives were also designed.

The new K67 derivatives were synthesized from commercially available 4-nitro-1-naphthylamine via 5 steps according to our previous method with a slight modification (Scheme 1) [18]. Benzenesulfonyl chlorides were purchased or synthesized from the corresponding substituted benzenes according to the method reported in the literature [18]. *para*-Methoxybenzyl acetoacetate was prepared from methyl acetoacetate and *para*-methoxybenzylalcohol [19]. Compound **1** was prepared from 4-nitro-1-naphthylamine and was condensed with the corresponding benzenesulfonyl chlorides (**2a**-**n**) followed by oxidation using ammonium cerium(IV) nitrite to give compounds **3a**-**n**. The diimine-type compounds **3a**-**f** and **3h**-**n** were added to the *para*-methoxybenzyl acetoacetate to obtain **4a**-**f** and **4h**-**n**, and then deprotection of the *para*-methoxybenzyl group with trifluoroacetic acid yielded compounds **5a**-**f** and **5h**-**n** with moderate overall yields (Scheme 1). In the case of **5g**, benzyl acetoacetate was added instead of *para*-methoxybenzyl acetoacetate to the diimine compound **3g,** and then, three benzyl groups were deprotected by hydrogeneration (Scheme 2). The synthetic compounds used for biological assays were recrystallized from suitable solvents.

Inhibitory activity against protein-protein interactions between Keap1 and p-p62 or Nrf2

The PPI inhibitory activities of the K67 derivatives were evaluated using a FP assay according to our previous method[17]. Compounds **5c**, **5e**, **5f**, **5j**, **5k** and **5l** had Clog*P* values over 4.5 (Table) and were too insoluble to measure their precise IC_{50} values. Other derivatives, except **5h**, showed IC_{50} values in the low μM range against both of the PPIs (Table). There was not much difference among the derivatives in terms of their PPI inhibitory activities (Keap1-*p*-p62/Keap1-Nrf2, the range was >1.3~2.2). Compound **5h**, which possesses nonsubstituted benzenesulfonamide, demonstrated the lowest inhibitory activity among the tested compounds.

Effect of the K67 derivatives on the sensitivity to anticancer agents in human hepatocellular carcinoma cell lines

In our previous study, K67 increased the sensitivity to sorafenib in Huh-1 cells that accumulate high levels of *p*-p62 [16]. Therefore, the effect of the newly synthesized K67 derivatives on the sensitivity to sorafenib was examined using Huh-1. For the purpose of comparison, the effect on Huh-7 cells in which p62 is not overexpressed was also evaluated. According to the previous method [16], after pre-incubation with the K67 derivatives (10 μM) for 72 hr, sorafenib (2.5 μM) was added to the medium, and the cells were incubated for another 72 hr. Then, cell viability was determined using a WST-8 assay.

Sorafenib (2.5 μM) decreased cell viability in both Huh-7 and Huh-1 cells compared to the control, but Huh-1 cells were more resistant to sorafenib than Huh-7 cells (Figure 2A). Co-incubation with the derivatives, except **5c** and **5f,** and sorafenib had no effect on viability of the Huh-7 cells. Under this condition, the propoxy derivative **5c** and the isopropoxy derivative **5d** decreased cell viability to approximately 40% in Huh-1 cells, whereas K67 (**5b**) and the methoxy derivative **5a** did not affect the sensitivity to sorafenib in this case (Figure 2A). It should be noted that compounds **5a**-**5d** showed no toxicity against both Huh-7 and Huh-1 cells when these compounds were added without sorafenib (Figure 3). Both the butoxy derivative **5e** and the isobutoxy derivative **5f** decreased the viability of Huh-1 cells by co-treatment with sorafenib (Figure. 2A); however, these derivatives decreased viability in both Huh-7 and Huh-1 cells even in the absence of sorafenib (Figure 3). The hydroxy derivative **5g** and the nonsubstituted derivative **5h** did not increase sorafenib sensitivity against Huh-1 cells (Figure. 2A). For the alkyl derivatives, compounds **5j**, **5k** and **5l** demonstrated significant effects, although the methyl derivative **5i** did not affect the sensitivity to sorafenib (Figure 2A). The chloro derivative **5m** and the acetamide derivative **5n** also increased the sensitivity to sorafenib (Figure 2A). Single administration of compounds **5g**-**5n** to both of the cell lines did not suppress cell viability (Figure 3).

Next, compound **5d**, which showed the most potent effect for overcoming sorafenib resistance in Huh-1 cells without any influence on Huh-7 cells, was evaluated for dose-dependency and compared with the original compound K67 (**5b**). K67 showed a significant effect against Huh-1 cells at over 50 μM, but the effect was weak (Figure 2B). On the other hand, **5d** tended to suppress Huh-1 cell proliferation at 1 μM and showed a significant effect at over 5 μM (Figure 2C). No synergistic effect was observed when Huh-7 cells were exposed to K67 or **5d** in combination with sorafenib (Figure 2B and C).

Moreover, we examined the effect of the K67 derivatives (10 μM) on the sensitivity to regorafenib, an alternative multikinase inhibitor, of Huh-1 cells (Figure 4). Compounds **5c**, **5d**, **5e** and **5f** significantly decreased viability of Huh-1 cells by co-treatment with regorafenib, similar to sorafenib, while other compounds, including K67 (**5b**), did not show any effect. Considering that **5e** and **5f** decreased cell viability in both Huh-7 and Huh-1 cells without regorafenib (Figure 3), it was suggested that only compounds **5c** and **5d** can overcome the resistance to regorafenib in Huh-1 cells.

Discussion

Overcoming chemoresistance is one of the key aspects in future cancer therapy not only from a perspective of improving prognosis but also from a perspective of reducing medical expenses [20]. In a previous study, we found K67 (**5b**) as the first-in-class compound that inhibits the PPI between *p*-p62 and Keap1 and increases the sorafenib-sensitivity of Huh-1 cells overexpressing *p*-p62 [16]. Therefore, the development of more effective anti-chemoresistance agents based on the structure of K67 is of great significance.

Although we had previously established the synthetic route for K67 in our previous report[17], a modification was made in the present study to efficiently prepare derivatives that have various substituents at the 4-position of the two benzensulfonamide groups. In particular, instead of benzyl acetoacetate, *para*-methoxybenzyl acetoacetate was added to the diimines, and then the *para*-methoxybenzyl group was deprotected with trifluoroacetic acid.

The Huh-1 cell line intrinsically accumulates phospho-S349 p62 [16]. Therefore, *p*-p62 competes with Nrf2 in binding to the Keap1 DC-domain and activates Nrf2 in Huh-1 cells, which induces cell progression and gain of chemoresistance. K67 (**5b**) increased the sensitivity to sorafenib in Huh-1 at 50 μM (Figure 2B) in agreement with our previous work[16]; however, 10 μM of K67 failed to decrease the Huh-1 cell viability under the conditions used in the present study (Figure

2A and 2B). On the other hand,the alkoxy derivatives **5c**, **5d**, **5e** and **5f** (10 μM) significantly increased the sensitivity of Huh-1 cells to sorafenib. These results suggest that elongation of the alkyl chain of the alkoxy groups could increase the sensitivity to sorafenib. The methoxy derivative **5a** had no effect, supporting the importance of alkyl chain length. However, **5e** and **5f** decreased the viability of both Huh-7 and Huh-1 cells in the absence of sorafenib, which means that the observed synergistic effects of sorafenib in combinationwith **5e** or **5f** in the Huh-1 cells were due to the toxicity of the compounds themselves and not due to increasing the sensitivity to sorafenib.

As for other derivatives, including the alkyl derivatives, compounds **5j**, **5k** and **5l** showed significant effects, while the methyl derivative **5i** did not affect the sensitivity to sorafenib. The chloro derivative **5m** and the acetamide derivative **5n** also increased the sensitivity to sorafenib. Thus, the 4-position of the benzenesulfonyl rings seemed to be a very important moiety to increase the sensitivity to sorafenib in Huh-1 cells.

The results of the current study showed that the selectivity between Keap1-*p*-p62 and the Keap-Nrf2 PPI inhibitory activities of the K67 derivatives had no correlation with the effect of increasing the sorafenib sensitivity in cellular assays. The comparison of the IC^{50} values evaluated by a simple FP assay using peptide fragments is probably inadequate to estimate the chemo-sensitizing effect in a cell-based assay that involves interactions at multiple levels. Although K67 (50 μM) clearly decreased the mRNA level of Nrf2-target proteins in our previous study [16], it is also possible that there is a difference between K67 (**5b**) and **5c-f** in regard to the mechanism of increasing sensitivity to sorafenib in Huh-1 cells. Thus, further investigations are required in order to clarify the mechanism of action of the new derivatives.

Compounds **5c**, **5d**, **5e** and **5h** also increased the sensitivity of Huh-1 cells to regorafenib, a second-line treatment agent for sorafenib-refractory HCC, which suggests that regorafenib-resistance in Huh-1 cells occurs via a similar mechanism to sorafenib-resistance, and patients with HCC in which p62 is overexpressed cannot achieve remarkable outcomes from treatment with regorafenib. Thus, the K67 derivatives newly synthesized in the present study may be novel therapeutics for highly advanced HCC.

Sorafenib not only inhibits various kinases but also induces ferroptosis, a novel type of regulated cell death[21]. Ferroptosis is characterized by iron-dependent lipid peroxidation-induced cell death that is not inhibited by the apoptosis inhibitor ZVAD-FMK[22]. In a ferroptotic cell, iron accumulation generates reactive oxygen species followed by lethal lipid peroxidation [23]. Sorafenib induces ferroptosis by the inhibition of cysteine/glutamate antiporters in the same way as erastin, a known ferroptosis inducer [24]. The activation of Nrf2 is one of the factors involved in ferroptosis-resistance, and indeed, Nrf2 suppression using shRNA enhanced the growth inhibitory activity of sorafenib against HCC cell lines, and this phenomenon was attenuated by ferrostatin-1, a selective ferroptosis inhibitor [25]. K67 derivatives may alter the response to sorafenib in Huh-1 cells by Nrf2-inactivation via the inhibition of the *p*-p62-Keap1 PPI followed by the induction of ferroptotic cell death. To the best of our knowledge, it has never been reported that regorafenib induces ferroptosis, but considering the structural similarity between sorafenib and regorafenib, a ferroptotic response might also be involved in the effect of K67 derivatives on the sensitivity to regorafenib. Further investigation of the possible molecular mechanisms underlying the anti-chemoresistance effect of K67 derivatives is needed.

In conclusion, we designed and synthesized novel K67 derivatives that possess *p*-p62-Keap1 PPI inhibitory activities and revealed their anti-chemoresistance effect in HCC. Among the derivatives, **5d** showed the strongest effect for a p62-overexpressing Huh-1 cell line without showing any synergistic effect in Huh-7, suggesting that **5d** might be a lead-compound for epoch-making anticancer agents. Our prospects for the future are to develop a more drug-like compound based on **5d**.

Funding

This research was supported by the Platform Project for Supporting in Drug Discovery and Life Science Research (Platform for Drug Discovery, Informatics, and Structural Life Science) from the Japan Agency for Medical Research and Development (AMED) and JSPS KAKENHI Grant Number 19K16322 and 18H02611.

Acknowledgement

We thank Taichi Iwai, Taketo Yoshida, Akihiro Yuasa and Mao Nakajima for their cooperation in the experiments.

References

1 (a) Chitapanarux T, Phormphutkul K. Risk Factors for the Development of Hepatocellular Carcinoma in Thailand. J. Clin. Transl. Hepatol. 2015;3:182-188. (b) Kar P. Risk Factors for Hepatocellular Carcinoma in India. J. Clin. Exp. Hepatol. 2014;4:S34-S42. (c) Fujiwara N, Friedman SL, Goossens N, Hoshida Y. Risk factors and prevention of hepatocellular carcinoma in the era of precision medicine. J. Hepatol. 2018;68: 526-549.

2 Raza A, Sood GK. Hepatocellular carcinoma review: Current treatment, and evidence-based medicine. World J. Gastroenterol. 2014;20:4115-4127.

3 Gong X, Qin S. Progress in systemic therapy of advanced hepatocellular carcinoma. World J. Gastroenterol. 2016;22:6582-6594.

4 Yang S, Liu G. Targeting the Ras/Raf/MEK/ERK pathway in hepatocellular carcinoma. Oncol. Lett. 2017;13:1041-1047.

5 Liu J, Liu Y, Meng L, Liu K, Ji B. Targeting the PD-L1/DNMT1 axis in acquired resistance to sorafenib in human hepatocellular carcinoma. Oncol. Rep. 2017;38:899-907.

6 Saeki I, Yamasaki T, Maeda M, Hisanaga T, Iwamoto T, Fujisawa K, Matsumoto T, Hidaka I, Marumoto Y, Ishikawa T, Yamamoto N, Suehiro Y, Takami T, Sakaida I. Treatment strategies for advanced hepatocellular carcinoma: Sorafenib vs hepatic arterial infusion chemotherapy. World J. Hepatol. 2018;10:571-584.

7 Taniguchi K, Yamachika S, He F, Karin M. p62/SQSTM1- Dr. Jekyll and Mr. Hyde that prevents oxidative stress but promotes liver cancer, FEBS Lett. 2016;590:2375-2397.

8 Rogov V, Dötsch V, Johansen T, Kirkin V. Interactions between Autophagy Receptors and Ubiquitin-like Proteins Form the Molecular Basis for Selective Autophagy. Mol. Cell2014;53:167-178.

9 Islam MA, Sooro MA, Zhang P. Autophagic Regulation of p62 is Critical for Cancer Therapy. Int. J. Mol. Sci. 2018;19:E1405

10 Komatsu M, Kurokawa H, Waguri S, Taguchi K, Kobayashi A, Ichimura Y, Sou YS, Ueno I, Sakamoto A, Tong KI, Kim M, Nishito Y, Iemura S, Natsume T, Ueno T, Kominami E, Motohashi H, Tanaka K, Yamamoto M. The selective autophagy substrate p62 activates the stress responsive transcription factor Nrf2 through inactivation of Keap1. Nat. Cell. Biol. 2010;12:213-23.

11 (a) Prestera T, Talalay P, Alam J, Ahn YI, Lee PJ, Choi AMK. Parallel induction of heme oxygenase-1 and chemoprotective phase 2 enzymes by electrophiles and antioxidants: Regulation by upstream antioxidant-responsive elements (ARE). Mol. Med. 1995;1:827-837, (b) Wild AC, Moinova HR, Mulcahy RT. Regulation of γ-Glutamylcysteine Synthetase Subunit Gene Expression by the Transcription Factor Nrf2. Biol. Chem. 1999;274:33627-33636, (c) Yates SM, Tran QT, Dolan PM, Osburn WO, Shin S, McCulloch CC, Silkworth JB, Taguchi K, Yamamoto M, Williams CR, Liby KT, Sporn SB, Sutter TR, Kensler TW. Genetic versus chemoprotective activation of Nrf2 signaling: overlapping yet distinct gene expression profiles between Keap1 knockout and triterpenoid-treated mice. Carcinogenesis, 2009;30:1024-1031, (d) Mitsuishi Y, Taguchi K, Kawatani Y, Shibata T, Nukiwa T, Aburatani H, Yamamoto M, Motohashi H. Nrf2 Redirects Glucose and Glutamine into Anabolic Pathways in Metabolic Reprogramming. Cencer Cell, 2012;22:66-79.

12 McMahon M, Itoh K, Yamamoto M, Hayes JD. Keap1-dependent proteasomal degradation of transcription factor Nrf2 contributes to the negative regulation of antioxidant response element-driven gene expression. J Biol Chem. 2003;278:21592-21600.

13 Zhang DD, Hannink M. Distinct Cysteine Residues in Keap1 Are Required for Keap1-Dependent Ubiquitination of Nrf2 and for Stabilization of Nrf2 by Chemopreventive Agents and Oxidative Stress. Mol. Cell. Biol, 2003;22:8137-8151.

14 Pallesen JS, Tran KT, Bach A. Non-covalent Small-Molecule Kelch-like ECH-Associated Protein 1-Nuclear Factor Erythroid 2-Related Factor 2 (Keap1-Nrf2) Inhibitors and Their Potential for Targeting Central Nervous System Diseases. J. Med. Chem. 2018;61:8088-8103.

15 Ichimura Y, Waguri S, SouY, Kageyama S, Hasegawa J, Ishimura R, Saito T, Yang Y, Kouno T, Fukutomi T, Hosii T, Hirao A, Takagi K, Mizusima T, Motohashi H, Lee MS, Yoshimoti T, Tanaka K, Yamamoto M, Komatsu M. Phosphorylation of p62 Activates the Keap1-Nrf2 Pathway during Selective Autophagy. Mol. Cell, 2013;51:618-631.

16 Saito T, Icimura Y, Taguchi K, Suzuki T, Mizushima T, Takagi K, Hirose Y, Nagahashi M, Iso T, Fukutomi T, Ohishi M, Endo K, Uemura T, Nishito Y, Okuda S, Obata M. Kouno T, Imamura R, Tada Y, Obata R, Yasuda D, Takahashi K, Fujimura T, Pi J, Lee M, Ueno T, Ohe T, Mashino T, Wakai T, Kojima H, Okabe T, Nagano T, Motohashi H, Waguri S, Soga T, Yamamoto M, Tanaka K. Komatsu M. p62/Sqstm1 promotes malignancy of HCV-positive hepatocellular carcinoma through Nrf2-dependent metabolic reprogramming. Nat. Commun, 2016;7:12030.

17 Yasuda D, Nakajima M, Yuasa A, Obata R, Takahashi K, Ohe T, Ichimura Y, Komatsu M, Yamamoto M, Imamura R, Kojima H, Okabe T, Nagano T, Mashino T. Synthesis of Keap1-phosphorylted p62 and Keap1-Nrf2 protein-protein interaction inhibitors and their inhibitory activity. Bioorg. Med. Chem. Lett. 2016;26:5956-5959.

18 Liu P, Du Y, Song L, Shen J, Li Q. Novel, potent, selective and cellular active ABC type PTP1B inhibitors containing (methanesulfonyl-phenyl-amino)-acetic acid methyl ester phosphotyrosine mimetic. Bioorg. Med. Chem. 2015;23:7079-7088.

19 Xu X, Wang X, Zavali PY, Doyle MP. Straightforward Access to the [3.2.2]Nonatriene Structural Framework via Intramolecular Cyclopropenation/Buchner Reaction/Cope Rearrangement Cascade. Org. Lett. 2015;17:790-793.

20 Nishimura K, Tsuchiya Y, Okamoto H, Ijichi K, Gosho M, Fukuyama M, Yoshikawa K, Ueda H, Bradford CR, Carey TE, Ogawa T. Identification of chemoresistant factors by protein expression analysis with iTRAQ for head and neck carcinoma, British J. Cancer. 2014;111:799-806.

21 Yang WS, Stockwell BS. Ferroptosis: Death by Lipid Peroxidation, Trends Cell Biol. 2016;26:165-176.

22 Dixon SJ, Lemberg KM,. Lamprecht MR, Skouta R, Zaitsev EM, Gleason CE, Patel DN, Bauer AJ, Cantley AM, Yang WS, Morrison III B, Stockwell BR. Ferroptosis: An Iron-Dependent Form of Nonapoptotic Cell Death. Cell. 2012;149:1060-1072.

23 Xie Y, Hou W, Song X, Yu Y, Huang J, Sun X, Kang R, Tang D. Ferroptosis: process and function. Cell Death Different. 2016;23:369-379.

24 Yu H, Guo P, Xe X, Wang Y, Chen G. Ferroptosis, a new form of cell death, and its relationships with tumourous diseases. J. Cell. Mol. Med. 2017;21:648-657.

25 Sun X, Ou X, Chen R, Niu X, Chen D, Kang R, Tang D. Activation of the p62-Keap1-NRF2 pathway protects against ferroptosis in hepatocellular carcinoma cells. Hepatology. 2016;63:173-184.

Table The PPI inhibitory activities and Clog*P* values of the K67 derivatives

Compound	PPI inhibitory activity				Selectivity index (Nrf2/*p*-p62)	Clog*P*[b]
	Keap1-*p*-p62 IC_{50} (μM)	95% CI	Keap1-Nrf2 IC_{50} (μM)	95% CI		
5a	1.4	1.3-1.5	2.0	1.9-2.2	1.4	2.9
5b (K67)	1.2	1.1-1.3	2.6	2.1-3.3	2.2	3.6
5c	>3	–	>3	–	N.D.	4.6
5d	2.2	2.0-2.5	3.9	3.2-4.7	1.8	4.3
5e	N.D.[a]	–	N.D.	–	N.D.	5.4
5f	N.D.	–	N.D.	–	N.D.	5.4
5g	7.1	6.7-7.6	12	10.7-12.9	1.7	2.4
5h	13	12.0-13.8	20	17.0-22.7	1.5	3.2
5i	1.4	1.3-1.5	2.3	2.0-2.7	1.6	4.2
5j	2.3	2.0-2.6	>3	–	>1.3	5.0
5k	>10	–	>10	–	N.D.	5.8
5l	>10	–	>10	–	N.D.	5.7
5m	4.3	3.9-4.6	8.9	7.7-10.3	2.1	4.3
5n	1.0	0.97-1.1	1.5	1.4-1.7	1.5	1.0

[a]Not detected. [b]Calculated by ChemDraw® Professional 15.1

Schemes and Figures

Scheme 1

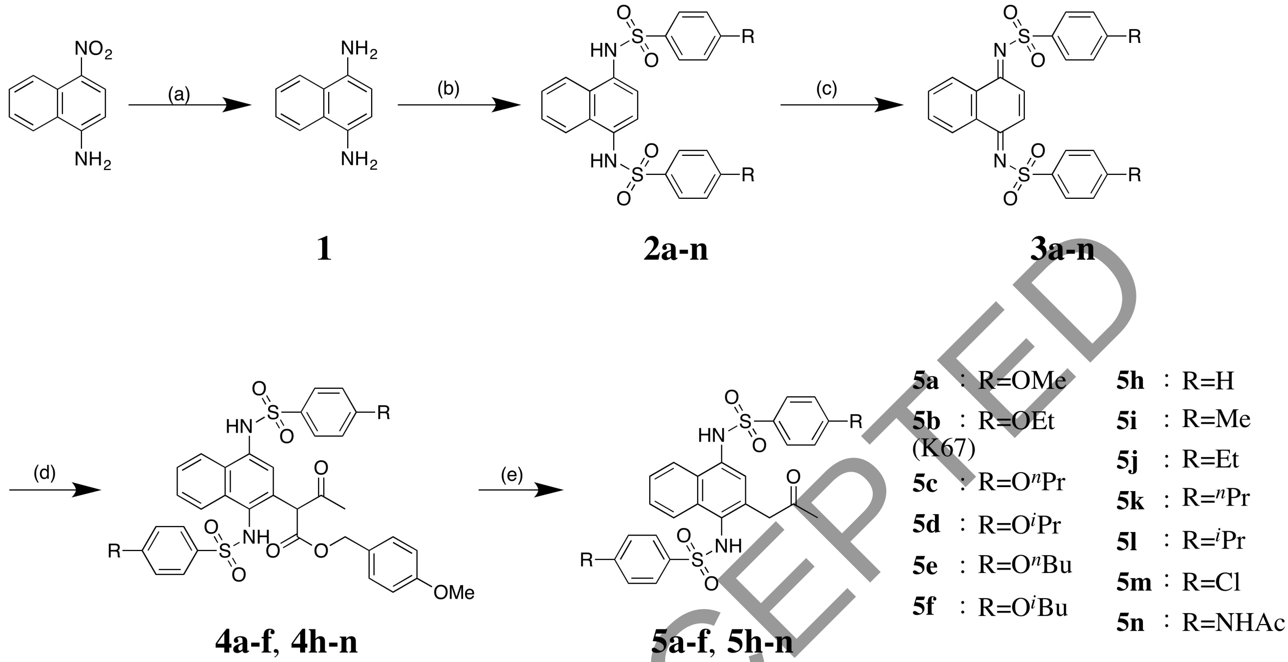

Scheme 2

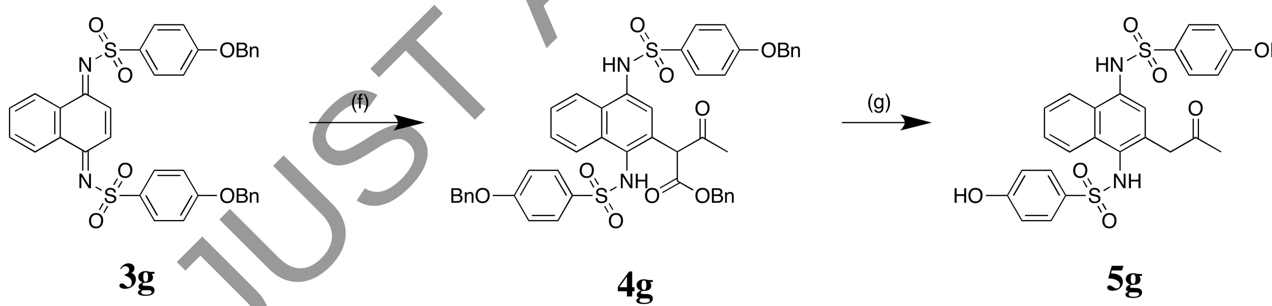

Figure 1

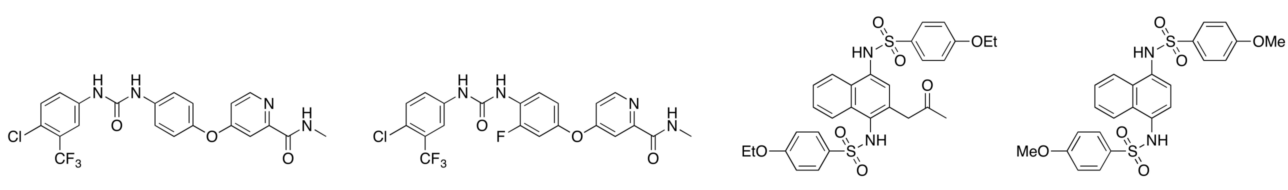

sorafenib regorafenib K67 Cpd16

Figure 2

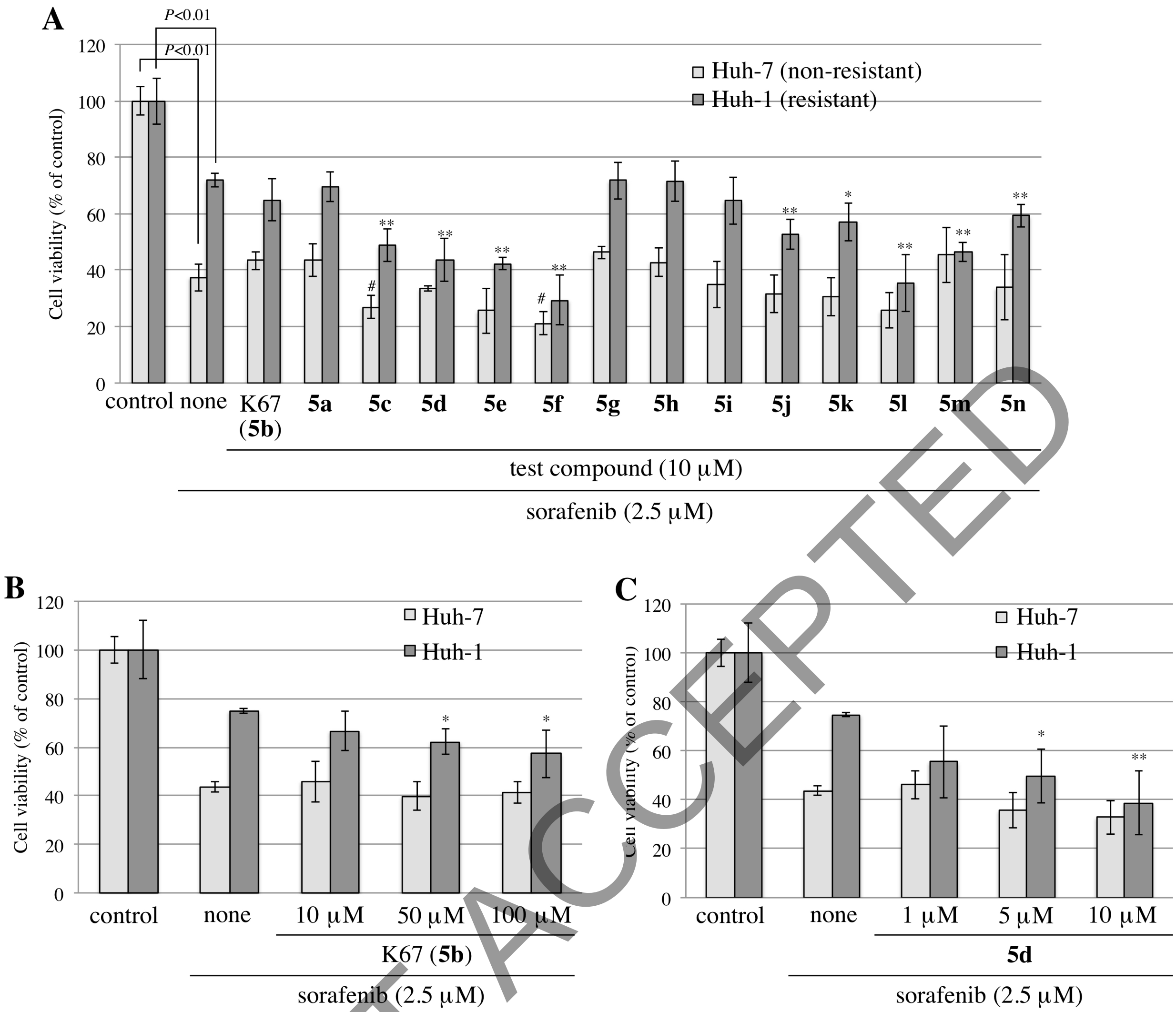
A
P<0.01
P<0.01
Cell viability (% of control)
120
100
80
60
40
20
0
Huh-7 (non-resistant)
Huh-1 (resistant)
control
none
K67 (5b)
5a
5c
5d
5e
5f
5g
5h
5i
5j
5k
5l
5m
5n
test compound (10 μM)
sorafenib (2.5 μM)
B
Huh-7
Huh-1
control
none
10 μM
50 μM
100 μM
K67 (5b)
sorafenib (2.5 μM)
C
Huh-7
Huh-1
control
none
1 μM
5 μM
10 μM
5d
sorafenib (2.5 μM)

Figure 3

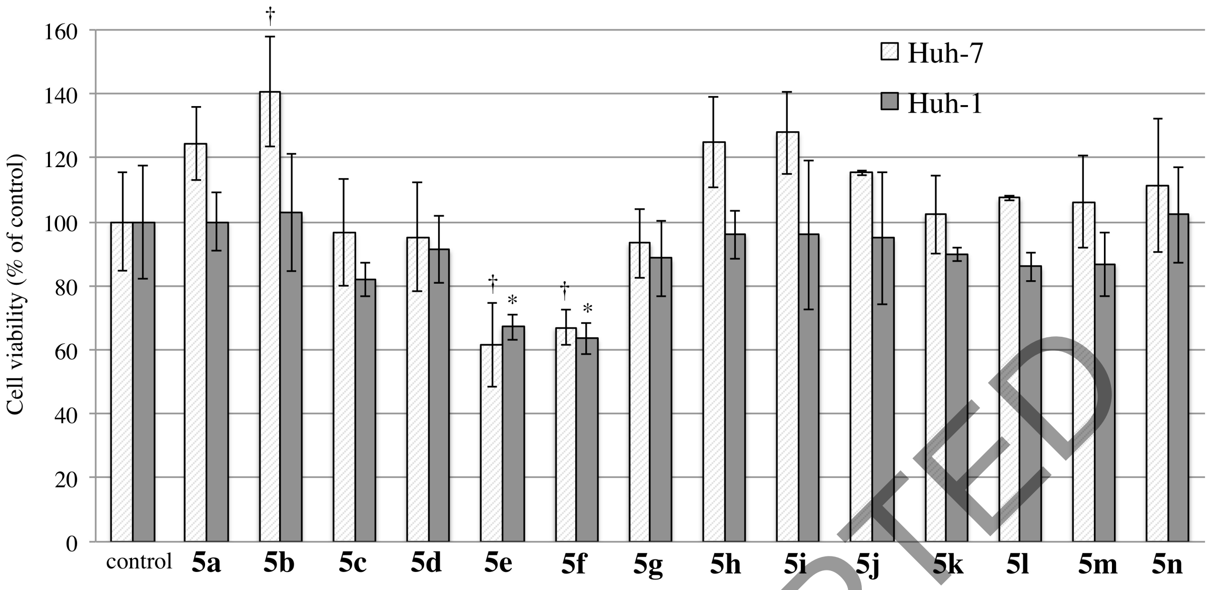

Figure 4

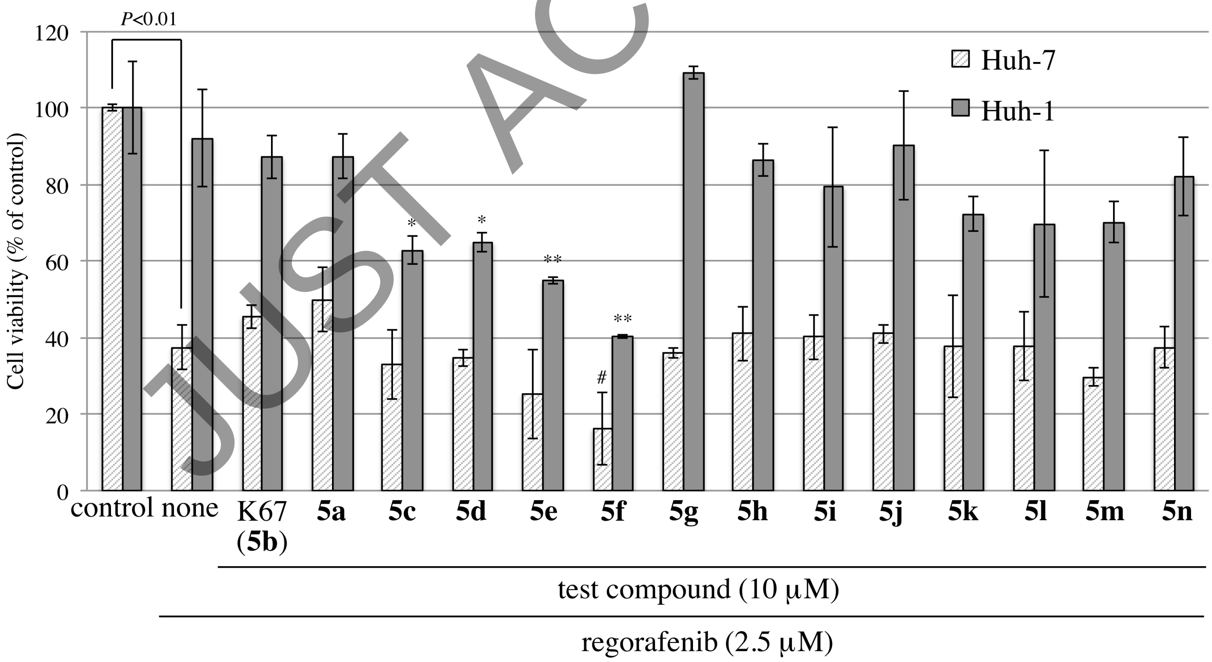

Scheme and Figure Captions

Scheme 1 Preparation of derivatives **5a-f** and **5h-n** (a) H^2, Pd/C, DCM, rt, 24 hr, 89%, (b) corresponding sulfonyl chloride, pyridine, DCM, rt, 2 hr, 80%-quant. (c) CAN, MeOH, rt, 30 min, (d) *p*-methoxybenzyl acetoacetate, TEA, toluene, 2 hr, (e) TFA, rt, 30 min, 34~69% for 3 steps.

Scheme 2 Preparation of derivative **5g**. Compound **3g** was prepared by CAN oxidation of a precursor compound synthesized from **1** and *para*-(benzyloxy)benzenesulfonyl chloride. (f) Benzyl acetoacetate, TEA, toluene, rt, 30 min, (g) H^2, Pd/C, DCM, rt, 24 hr, 38% yield for 2 steps.

Figure. 1 Structures of sorafenib, regorafenib, K67 and Cpd16

Figure 2 Effect of K67 derivatives on the sensitivity to anticancer agents. (**A**) Co-incubation with K67 derivatives (10 μM) and sorafenib (2.5 μM). Huh-1 (resistant) or Huh-7 (nonresistant) cells (5,000 cells/mL) were seeded onto 96-well microplates and precultured until adherent. After 24 hr, test compounds were added and incubated for 72 hr. Then, sorafenib was added and incubated for another 72 hr. Cell viability was determined using a WST-8 assay. (**B, C**) Dose-dependent effect of K67 (B) and **5d** (C) on the sensitivity to sorafenib of Huh-7 and Huh-1. Experiments were performed in a similar manner to that described for Figure. 2A. #; P<0.05 vs control (Huh-7), *P<0.05 vs control (Huh-1), **P<0.01 vs control (Huh-1). n=3.

Figure 3 Single treatment with K67 derivatives for Huh-1 and Huh-7. Huh-1 or Huh-7 cells (5,000 cells/mL) were seeded onto 96-well microplates and pre-cultured until adherent. After 24 hr, test compounds were added and incubated for 144 hr. Then, cell viability was determined using a WST-8 assay (n=3).

Figure 4 Co-incubation with K67 derivatives (10 μM) and regorafenib (2.5 μM). Experiments were performed in a similar manner to that described for Figure. 2A. #; P<0.05 vs control (Huh-7), *P<0.05 vs control (Huh-1), **P<0.01 vs control (Huh-1). n=3.

Table The PPI inhibitory activities and Clog$P$ values of the K67 derivatives

Compound	PPI inhibitory activity				Selectivity index (Nrf2/*p*-p62)	Clog*P*[b]
	Keap1-*p*-p62 IC_{50} (μM)	95% CI	Keap1-Nrf2 IC_{50} (μM)	95% CI		
5a	1.4	1.3-1.5	2.0	1.9-2.2	1.4	2.9
5b (K67)	1.2	1.1-1.3	2.6	2.1-3.3	2.2	3.6
5c	>3	–	>3	–	N.D.	4.6
5d	2.2	2.0-2.5	3.9	3.2-4.7	1.8	4.3
5e	N.D.[a]	–	N.D.	–	N.D.	5.4
5f	N.D.	–	N.D.	–	N.D.	5.4
5g	7.1	6.7-7.6	12	10.7-12.9	1.7	2.4
5h	13	12.0-13.8	20	17.0-22.7	1.5	3.2
5i	1.4	1.3-1.5	2.3	2.0-2.7	1.6	4.2
5j	2.3	2.0-2.6	>3	–	>1.3	5.0
5k	>10	–	>10	–	N.D.	5.8
5l	>10	–	>10	–	N.D.	5.7
5m	4.3	3.9-4.6	8.9	7.7-10.3	2.1	4.3
5n	1.0	0.97-1.1	1.5	1.4-1.7	1.5	1.0

[a]Not detected. [b]Calculated by ChemDraw® Professional 15.1

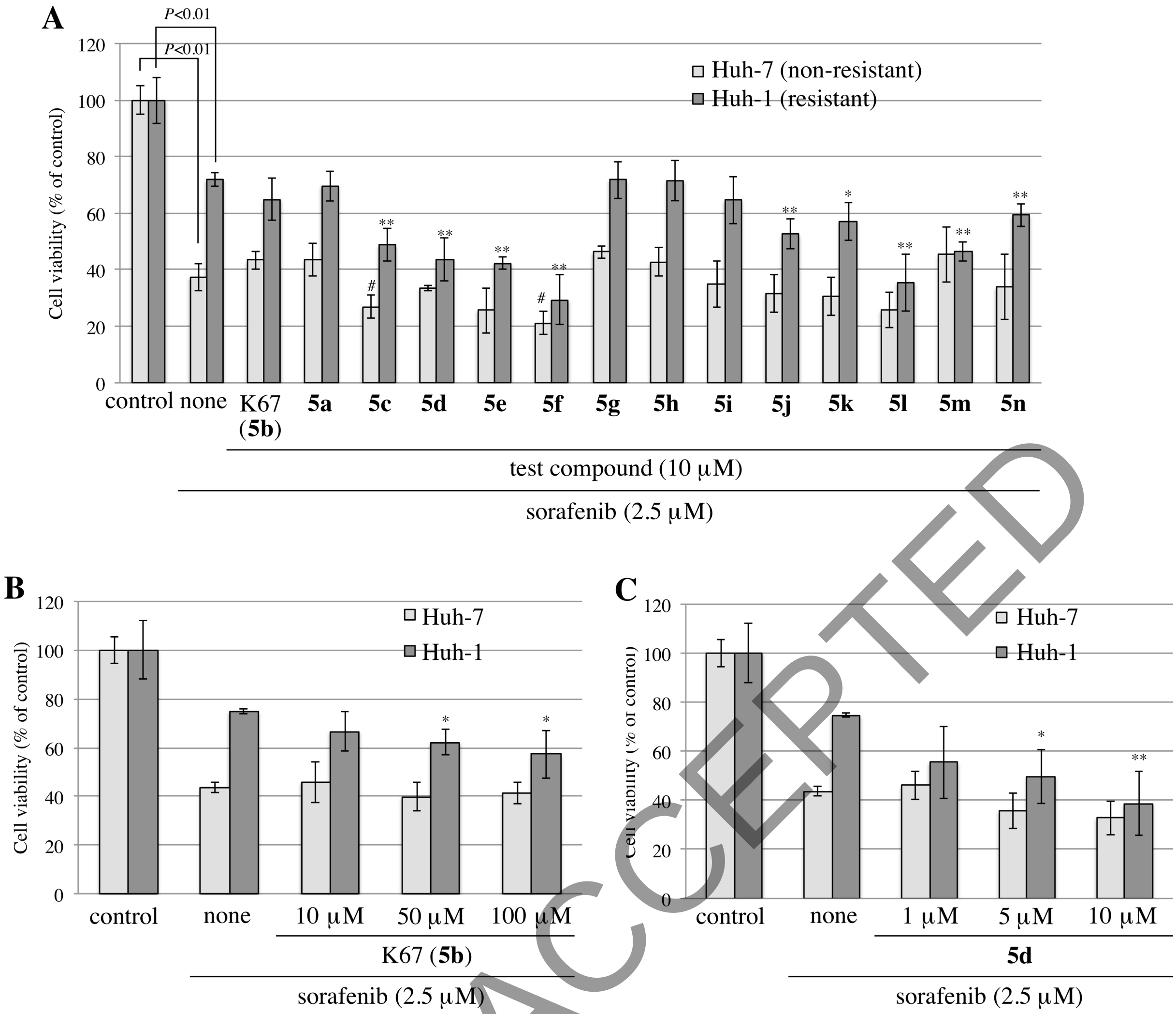

A
P<0.01
P<0.01
Huh-7 (non-resistant)
Huh-1 (resistant)
Cell viability (% of control)
control
none
K67 (5b)
5a
5c
5d
5e
5f
5g
5h
5i
5j
5k
5l
5m
5n
test compound (10 μM)
sorafenib (2.5 μM)
B
Huh-7
Huh-1
Cell viability (% of control)
control
none
10 μM
50 μM
100 μM
K67 (5b)
sorafenib (2.5 μM)
C
Huh-7
Huh-1
Cell viability (% of control)
control
none
1 μM
5 μM
10 μM
5d
sorafenib (2.5 μM)

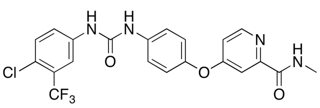

sorafenib

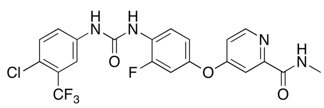

regorafenib

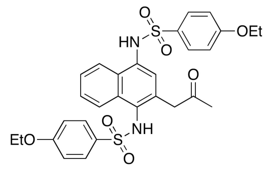

K67

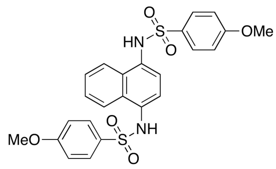

Cpd16

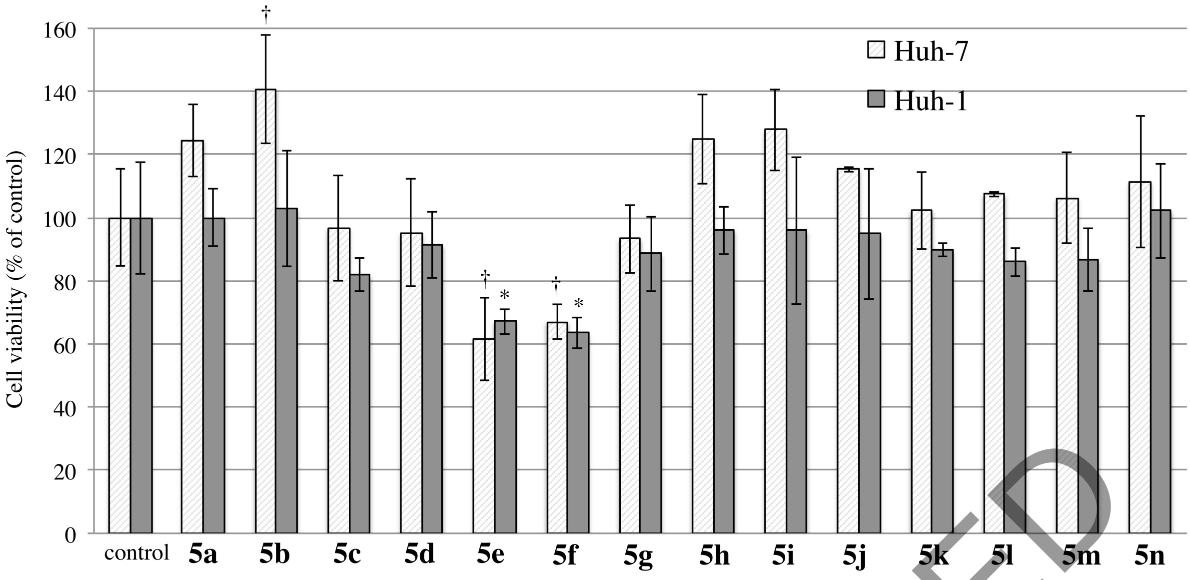

Cell viability (% of control)
160
140
120
100
80
60
40
20
0
Huh-7
Huh-1
control
5a
5b
5c
5d
5e
5f
5g
5h
5i
5j
5k
5l
5m
5n
†
*

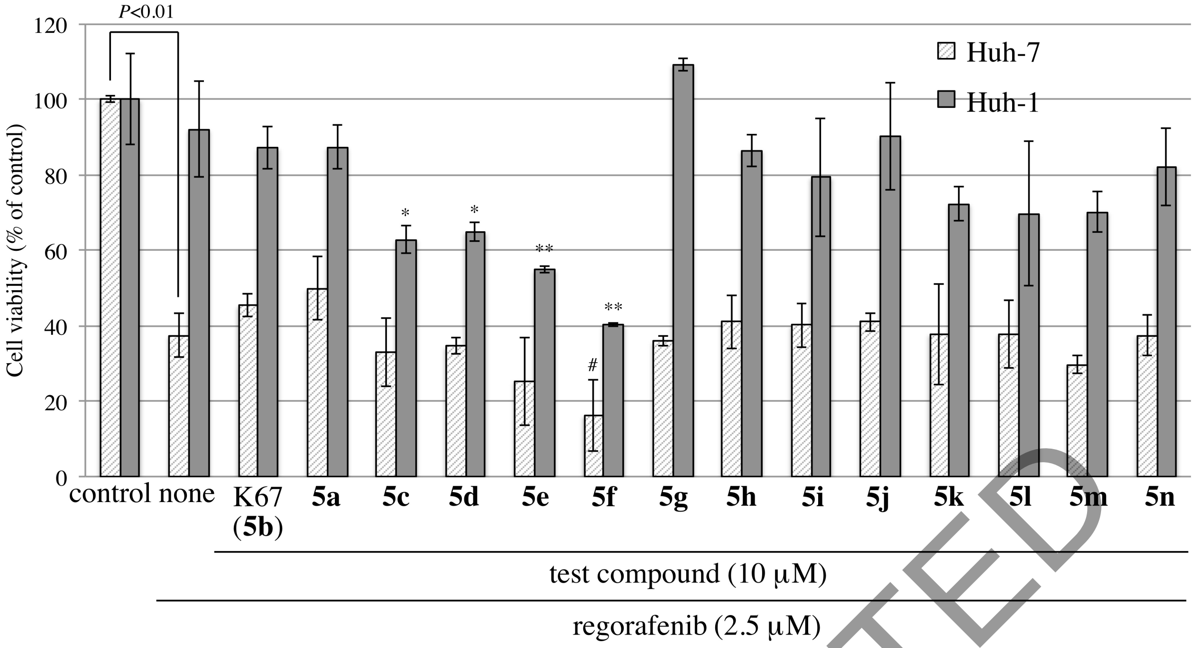

P<0.01
Cell viability (% of control)
120
100
80
60
40
20
0
Huh-7
Huh-1
*
*
**
**
#
control
none
K67 (5b)
5a
5c
5d
5e
5f
5g
5h
5i
5j
5k
5l
5m
5n
test compound (10 μM)
regorafenib (2.5 μM)

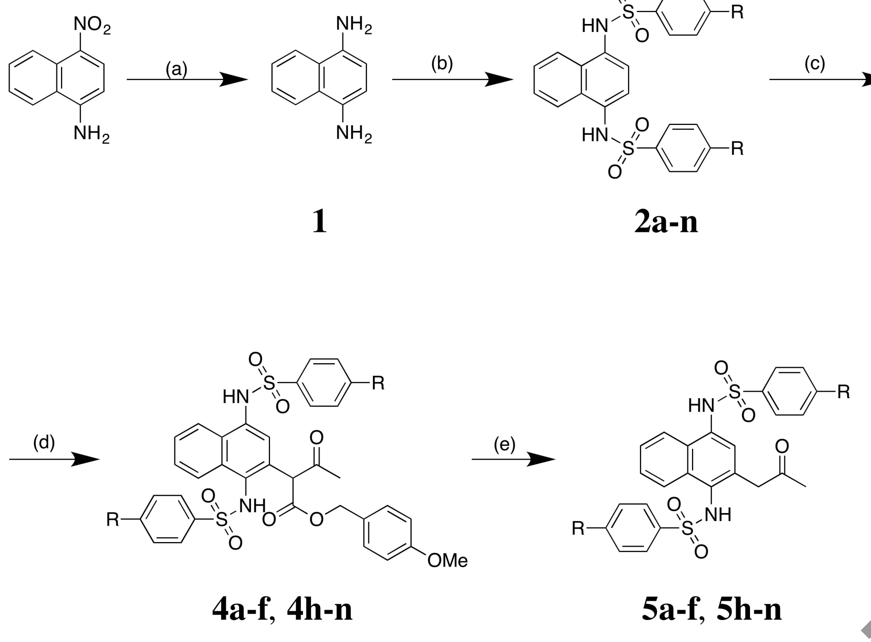

5a ：R=OMe
5b ：R=OEt (K67)
5c ：R=O^{n}Pr
5d ：R=O^{i}Pr
5e ：R=O^{n}Bu
5f ：R=O^{i}Bu
5h ：R=H
5i ：R=Me
5j ：R=Et
5k ：R=^{n}Pr
5l ：R=^{i}Pr
5m ：R=Cl
5n ：R=NHAc

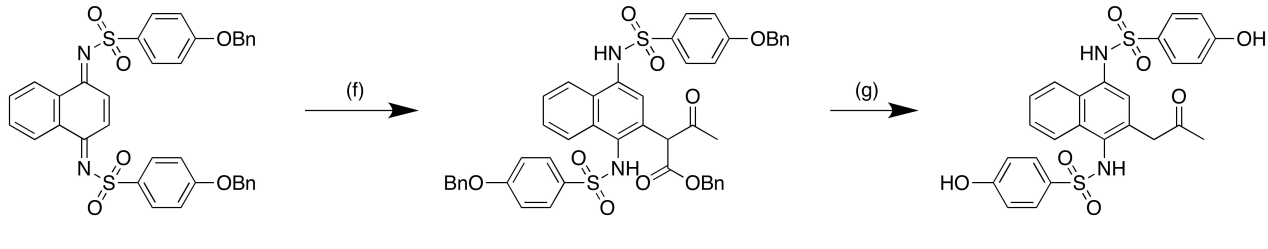

3g **4g** **5g**